ANNUAL REVIEWS

Annual Review of Earth and Planetary Sciences

Moist Heat Stress on a Hotter Earth

Jonathan R. Buzan[1,2] and Matthew Huber[1]

[1]Department of Earth, Atmospheric, and Planetary Sciences, Purdue University, West Lafayette, Indiana 47907, USA; email: huberm@purdue.edu

[2]Climate and Environmental Physics, Physics Institute and Oeschger Centre for Climate Change Research, University of Bern, Bern 3012, Switzerland

Annu. Rev. Earth Planet. Sci. 2020. 48:623–55

First published as a Review in Advance on February 21, 2020

The *Annual Review of Earth and Planetary Sciences* is online at earth.annualreviews.org

https://doi.org/10.1146/annurev-earth-053018-060100

Keywords

heat stress, heat waves, climate extremes, climate dynamics, food-energy-water security, limits to habitability

Abstract

As the world overheats—potentially to conditions warmer than during the three million years over which modern humans evolved—suffering from heat stress will become widespread. Fundamental questions about humans' thermal tolerance limits are pressing. Understanding heat stress as a process requires linking a network of disciplines, from human health and evolutionary theory to planetary atmospheres and economic modeling. The practical implications of heat stress are equally transdisciplinary, requiring technological, engineering, social, and political decisions to be made in the coming century. Yet relative to the importance of the issue, many of heat stress's crucial aspects, including the relationship between its underlying atmospheric drivers—temperature, moisture, and radiation—remain poorly understood. This review focuses on moist heat stress, describing a theoretical and modeling framework that enables robust prediction of the averaged properties of moist heat stress extremes and their spatial distribution in the future, and draws some implications for human and natural systems from this framework.

- Moist heat stress affects society; we summarize drivers of moist heat stress and assess future impacts on societal and global scales.
- Moist heat stress pattern scaling of climate models allows research on future heat waves, infrastructure planning, and economic productivity.

1. INTRODUCTION

Heat stress: a situation where the body is overwhelmed by metabolic heat production, which can lead to runaway temperature increases in the body's core

Heat waves kill on massive scales. The 2003 European heat waves caused widespread deaths due to prolonged and repeated exposure to heat stress (Beniston 2004). An estimated 40,000 people died during several weeks in August (Garcia-Herrera et al. 2010) and possibly tens of thousands more altogether for the entire summer period (Robine et al. 2008). The deadliest heat wave on record was the 2010 heat wave in Russia, which killed in excess of 55,000 (Barriopedro et al. 2011, Dole et al. 2011). Killer heat waves are the pointy end of the spear that more and more frequently prods us to recognize that the hot tail of modern climate distributions can be harmful or even lethal.

More broadly, heat stress is well established as a leading cause of weather-related deaths (Barriopedro et al. 2011, Buzan et al. 2015), and it is increasingly linked to complex social impacts, such as crime, strife, conflict, reduced educational attainment, morbidity, and reduced labor productivity (Burke et al. 2009, Kelley et al. 2015, Schleussner et al. 2016, Mora et al. 2017a, Randell & Gray 2019), both now and in the future (Jendritzky & Tinz 2009, Sherwood & Huber 2010, Field et al. 2012, Seneviratne et al. 2012, Dunne et al. 2013, Houser et al. 2015, Hsiang & Sobel 2016, Kjellstrom et al. 2016, Hsiang et al. 2017). Indeed, all studies we are aware of have concluded that future warming will increase the prevalence of these hot and harmful conditions (Meehl & Tebaldi 2004, Diffenbaugh et al. 2007, Diffenbaugh & Ashfaq 2010, McCarthy et al. 2010, Sherwood & Huber 2010, Willett & Sherwood 2010, Fischer et al. 2012). These shifts in temperature distributions will come with a reduction in cold extremes, but the benefits of fewer extremely cold days do not cancel the increase in harm caused by hot extremes (Huber et al. 2017).

Moisture has been understood as a major element of heat stress since studies began (Haldane 1905, Brunt 1943), and heat stress is maximized during simultaneous high extremes of both temperature and humidity. Despite recognition that moisture is important, the study of moist heat stress as a distinct field within the broad field of heat stress has lagged. Because moist heat stress involves extrema of joint distributions of temperature and humidity—for which no general theory exists—studies are generally reliant on brute force predictions from climate models. Some global climate change studies have included heat stress metrics incorporating temperature-humidity covariance (Sherwood & Huber 2010, Willett & Sherwood 2010, Fischer & Knutti 2012, Smith et al. 2016), and this continues to be a rapidly developing field (Mora et al. 2017b, Russo et al. 2017). It is clear from this work that moist heat waves have notably different global- to synoptic-scale patterns (Buzan et al. 2015) and dynamics (Raymond et al. 2017) than dry ones and therefore require different conceptual models to understand and predict their mean state, trends, and variability.

Groundwork has been laid to develop a more theoretical approach emerging from thermodynamic and convective dynamical constraints for these temperature-humidity distributions (Sherwood & Huber 2010, Willett & Sherwood 2010, Fischer & Knutti 2012, Buzan et al. 2015, Matthews 2018). In this review we highlight the central role of moist convective dynamics in understanding heat stress and further develop these concepts, as well as frame their strengths and limitations, by evaluating moist thermodynamic variables within a host of general circulation models. In Section 2, we review the long-established physical basis demonstrating that heat stress on humans, and endotherms in general, can best be thought of from an energy balance framework that—just like Earth's surface energy budget—is a function of temperature, humidity, and radiative inputs. While we lightly touch on the biological, evolutionary, and medical foundations for these relations, and acknowledge the broader societal ramifications of this work, we can do little more than scratch the surface. In Section 3, we give a quick overview of the drivers of heat stress today. In Section 4, we cover the thermodynamic theory of moist heat stress and build toward a predictive conceptual framework. We explore a minimal thermodynamical model for the globally averaged behavior of heat stress extremes, compare them to observations, and expand the model

to include future projections of heat stress. In Section 5, we identify robust spatial patterns and hotspots of change and consider the impact of these changes on future labor capacity. In Section 6, we summarize leading issues and concerns for future research.

2. FUNDAMENTALS OF HEAT STRESS INCLUDING MOISTURE

2.1. The Human Heat Engine and Homeostasis

Humans—and other endotherms, e.g., placental mammals and birds—can fundamentally be thought of as heat engines that burn food to do work (Speakman & Król 2010, 2011). This metabolic process is exothermic and requires that they must consume food and water to feed the fire and, simultaneously, lose resulting metabolic heat. For example, metabolic heat is generated within the body's core and is dependent on levels of activity, from a basal metabolic rate up to ~10 times that of minimum heat production due to strenuous activity from work. Maintaining homeostasis is a complex process involving many interacting components involving endothermy. Endothermic animals must maintain core body temperatures within a narrow range, close to 37°C for humans. When confronted with heat stress, humans have a variety of systems that interact to cope with heat strain and attempt to preserve homeostasis (for mammals, see the sidebar titled Animal Models).

The hypothalamus, the portion of the brain responsible for the autonomic (peripheral) nervous system, regulates thermal control. Sensing core body temperatures using thermosensitive neurons, the hypothalamus releases or shuts off chemical compounds, which prompts the central nervous system (Platt & Vicario 2013) to induce multiple organs to react. In normal thermoregulation, as internal temperatures rise, the hypothalamus initiates vasodilation (dilation of the blood vessels) (Simon 1993) and also increases heart rate (Yokota et al. 2008). These processes promote internal heat transport to the skin as the hypothalamus simultaneously enhances sweating. For skin, heat transfer is dependent on the environment. There are four different methods of heat transport at the exterior of a human body (**Figure 1**): radiation, convection, conduction, and evaporation (Simon 1993, Koppe et al. 2004, Gaughan et al. 2009). As temperatures increase outside the human

Endothermy: physiological generation and regulation of body temperature by metabolic means; the property or state of being warm-blooded

Heat strain: the physiological response to the body accumulating heat during heat stress

Homeostasis: the tendency toward a relatively stable equilibrium between interdependent elements, especially as maintained by physiological processes

ANIMAL MODELS

Other mammals self-regulate their internal temperatures and have many strategies in place for dealing with heat stress (Tattersall et al. 2012, Mitchell et al. 2018); for this reason, they are often used as an analog to the human body in heat stress studies (Bynum et al. 1978, Hightower & Guidon 1989). Livestock and endothermic animals in general are negatively impacted by heat stress, leading to a reduction in feeding, meat yield, reproduction rates, milk yield, and egg laying as well as death (St-Pierre et al. 2003, Gaughan et al. 2013). Horses and cattle die when core temperatures reach ~43°C for extended periods of time (Gaughan et al. 2009), as do humans (Simon 1993). Some large ungulates (hoofed mammals) dilate specialized blood vessels (carotid retes) that run near the evaporative cooling areas around the head and neck, enhancing heat dissipation to keep the all-important brain cool. However, this process shuts down during excessive exercise, such as fight-or-flight responses, which can induce hyperthermia (Mitchell et al. 2002). Baboons living in strenuous hot environments can survive increased exposure to solar radiation, provided they have adequate access to water (Mitchell et al. 2009). When baboons suffer heat stroke, the resulting inflammatory response involving cytokine signaling molecules (Bouchama et al. 2005) is similar to humans' responses for heat stress (Mitchell et al. 2009). The data sets derived from the aforementioned studies are used to compare with and inform human heat stress models.

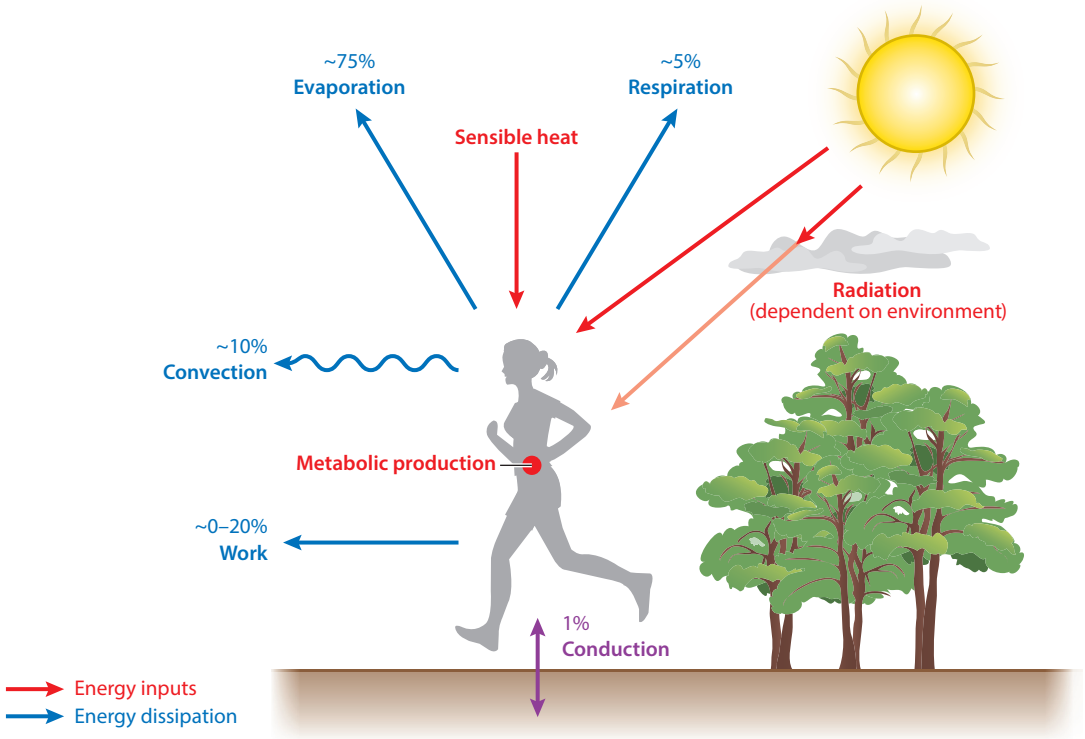

Figure 1

Energy balance in the human body. The red arrows represent the flux of energy into humans. The blue arrows are energy dissipation mechanisms and their relative contributions for humans: evaporation, respiration, convection, conduction (conduction may add heat and thus is *purple*), and work. The dissipation mechanisms are variable due to thermal inertia and may not reach steady state (quantities may not equal 100%).

body (a hot environment), the primary method of removing excess heat is through evaporation, which controls ~75% of heat loss (Koppe et al. 2004). However, if the local moisture conditions in the environment reduce the effectiveness of evaporation, the hypothalamus will not be able to regulate heat; at extreme temperature and moisture conditions, thermoregulation is impossible and heat stroke can ensue.

In the absence of heat dissipation, this metabolic heating would warm a resting person by >1°C per hour (Platt & Vicario 2013), so avoiding a slow sous vide cooking requires substantial heat loss. Heating directed toward the body from the atmosphere increases the body's overall heat load while also typically reducing the body's ability to maintain homeostasis. Heat stress occurs when environmental conditions overwhelm the body's cooling mechanisms, potentially leading to degraded work capacity, loss of homeostasis, and hyperthermia associated with a rapid increase in core body temperatures and degraded work capacity. A sustained increase of internal temperatures of ~3°C can lead to heat stroke and death (Simon 1993).

Heat load: the amount of energy required to maintain homeostasis

2.2. People Are Complicated

To frame the range of factors that define and affect the full spread of heat stress–related issues, we can draw on the medical and epidemiological heat stroke literature. Heat stroke is a

life-threatening condition that must be treated; even with treatment, mortality rates can reach 50%, and many survivors exhibit long-term neurological and multi-organ impairment (Koppe et al. 2004, Epstein & Moran 2006, Li et al. 2012). In a clinical setting heat stroke is defined as the core body temperature rising above 40°C and is accompanied by neurological symptoms (Koppe et al. 2004, Bouchama et al. 2005, Epstein & Moran 2006). Heat stroke is normally divided into two kinds: classic versus exertional heat stroke. This conceptual difference between classic and exertional heat stroke in the clinical literature maps imperfectly into future projections, but despite its imperfections, it provides key insights and is important to briefly summarize.

2.2.1. Classic heat stroke and vulnerable populations. Classic heat stroke occurs in the absence of physical exertion under basal metabolic heat generation and affects susceptible people: the very young and very old, those with chronic illness and/or taking a wide variety of common medications and drugs, specific ethnic groups, women, and those with lower socioeconomic status (Basu 2009, Kjellstrom et al. 2009a, Gonzalez et al. 2010). Because fatty tissues have about half the thermal conductivity of other tissues, obesity is also an important factor contributing to classic heat stress. As described eloquently by Margolis (2014), the impact of heat stress on populations is mediated by the full host of public health issues, including aging, chronic diseases, and obesity, as well as the investment in training and infrastructure to reduce vulnerability. Thus, a purely meteorological understanding of heat stress clearly has further deficiencies in terms of utility for concrete risk characterization, especially in the near term for those vulnerable to classic heat stroke.

For example, research on the Chicago heat wave in 1995 shows that mortality was heavily influenced by health status and the presence of air conditioning (Semenza et al. 1996). In analyzing demographics in cities, another study concluded that for the United States, mortality from heat falls disproportionately on the socially disadvantaged (O'Neill et al. 2003). One study analyzing hospital admissions found a significant relationship between temperature and hospital admissions rates (Li et al. 2012). Furthermore, Li et al. (2012) used late twenty-first-century climate projections to simulate the change in hospital admissions to determine the number of hospitals that may be impacted by climate change. Humans working in environments with chronic heat exposure may increase the incidence rate of heat-related morbidity. For example, chronic kidney disease rates—normally associated with diabetes—have substantially increased in Nicaragua (O'Donnell et al. 2011). However, numerous studies show that the factor linking the majority of cases is frequent exposure to high heat environments (Crowe et al. 2009, 2010; Delgado Cortez 2009; Ross et al. 2018). These results have generated efforts to characterize these high heat work environments (Sheffield et al. 2013). Future projections estimate that there will be a 15% increase in exposure to high heat stress days in the region.

2.2.2. Exertional heat stroke and fit, acclimated populations. Within the clinical literature, exertional heat stroke is associated with physical exertion that raises metabolic heat generation and requires an accompanying increase in heat loss to avoid heat stress. To facilitate efficient cooling of the core, the heart's blood pressure and flow rates increase or reduce depending on the environment, shunting heat to the skin to be evaporated. Healthy, hydrated, and acclimated individuals can survive unharmed and even perform labor at dry bulb temperatures higher than 50°C. A physically fit individual can produce up to 3 liters of sweat per hour (Koppe et al. 2004), providing adequate evaporative cooling under a wide range of conditions. This mechanism fails when high ambient humidity prevents efficient evaporation. Because the mechanism failure is associated with strenuous physical activity, it is commonly found even in healthy, fit teenagers and adults (including those accustomed to heavy labor), outdoor laborers, soldiers, and athletes.

The human body has the capacity to adapt to a variety of environments through acclimatization. Respiration rates, oxygen volume, and gas exchanges are heavily dependent on whether subjects are acclimatized (Pandolf & Kamon 1974). In the literature on exertional heat stress, a primary strategy for avoiding heat-related illness is to enable acclimatization. Acclimatization to heat can be accomplished relatively quickly with an e-folding timescale, which accomplishes about 75% of the final acclimatization within 6 days of heat stress exposure. Likewise, the human vascular system reacts to prolonged strenuous exposure (Koppe et al. 2004). If local temperatures increase, the human body reacts by increasing the density of blood vessels in the skin. Acclimatization is lost with a similar e-folding timescale when exposure to either exertion-related or passive heat stress is reduced (Whitman et al. 1997). It subsequently takes less time to regain acclimatization. Behavioral adaptation is also an important strategy (Oppermann et al. 2018, Day et al. 2019), such as shifting working hours.

2.2.3. Mapping these concepts to upper and lower tolerances for societies. If we think more broadly to whole populations within a global context, these clinical definitions provide two end-members of fitness and resilience to heat stress. Under low heat stress conditions, those who are most vulnerable will be susceptible to classic heat stroke and its less severe cousins. Morbidity and mortality in modern heat stress regimes are dominated by the features of classic heat stroke. This also means that empirical regression–based estimates of heat stress's impacts on health and well-being are likely capturing the unacclimated, unadapted response of the least healthy, least prepared, and least technologically buffered members of society. Such measures are thus necessarily biased toward overestimating the impact of heat stress when extrapolated to a warmer world. Echoes of this can be seen in the fact that the European heat wave of 2005 killed very few compared to 2003, despite being just as hot. But, at higher heat stress conditions, even the fit and acclimated can fall prey to what would today be classified as exertional heat stroke. The exertional heat stroke literature more accurately captures the limits of fit, adapted, and acclimated humans, likely providing more accurate and robust (i.e., not prone to substantial changes), but also overly optimistic, estimates of humans' ability to acclimate and adapt practices to heat stress induced by future climate change.

In-between those two end-members are a huge range of complicating and potentially mitigating or exacerbating factors (McGregor & Vanos 2018, Oppermann et al. 2018, Wang et al. 2018, Day et al. 2019). Sound science-based strategies can be used to adapt societies to a range of future heat extremes (Coffel et al. 2018). Existing technology can profoundly reduce heat stress either in the acute, emergency sense during heat waves in the form of public cooling centers or in the long term with widespread adoption of air conditioning (Azer & Hsu 1977b, Semenza et al. 1996, Cain 2006, Kovats & Hajat 2008, Li et al. 2012, Ito et al. 2018). Cooling techniques that rely on enhancing evaporative cooling, such as fans and swamp coolers, can play a useful role in reducing heat stress as well, but both have reduced efficacy as humidity increases and may even increase heat stress when temperatures are hot (>38°C) and humid [>35% relative humidity (RH)] (Jendritzky & Tinz 2009). Thus, when the focus is on moist heat waves, as it is here, air conditioning is of special value because it reduces both temperature and humidity. In a warmer world, air conditioning may become necessary for much of the world to survive, and consequently power outages may be deadly.

In this review, we primarily seek to understand broad and unchanging properties that lend themselves more to metrics most appropriate for the fit and acclimated, i.e., the upper bounds of what humans can withstand without technological assistance. But the limitations of this approach must be acknowledged. The choice of approaches and whether they underestimate risk versus overestimate risk are best left to the needs and drivers of individual investigations.

2.3. Selected Heat Stress Metrics and Their Applications

Human physiology is a complex system. Ideally one should use a well-tuned, well-validated prognostic model encompassing a sophisticated treatment of these processes to predict heat stress and its physiological responses (Stolwijk 1971, Kraning & Gonzalez 1997, Fiala et al. 1999). In practice, this is rarely done for meteorological and climate projection applications. Instead, prognostic physiological models are typically bypassed in favor of very simple, usually empirically based diagnostic metrics or indices. Over 120 diagnostic heat stress metrics have been developed (some of which are summarized in de Freitas & Grigorieva 2014, Buzan et al. 2015, and Gao et al. 2018).

Limitations to using these diagnostic indices to predict humans' physical response to heat stress include lack of a time-varying component, so they neglect sustained heat load. Each metric has a limited empirical scope, and comparative studies evaluating the relative merits of different metrics for global-scale climate projections are lacking. Many metrics are duplicative because they simply fit the same parameters using slightly different data sets; most neglect, or dramatically oversimplify, solar and thermal radiation to physiological heat stress (Bedford & Warner 1934, Minard et al. 1957, Kuehn et al. 1970, Liljegren et al. 2008). A combined metric accounting for all of these factors is the wet bulb globe temperature (WBGT), an empirical diagnostic index developed for the US military as a warning system to prevent heat stress casualties (Minard et al. 1957, Cain 2006) and commonly used in the health literature (Budd 2008, Liljegren et al. 2008). The International Organization for Standardization (ISO) has policies for measuring heat stress and determining workloads within workplace environments, such as ISO 7243, which uses the WBGT as the standard (Parsons 2006). The WBGT is not typically calculated explicitly in climate models, although simplified versions have been (Buzan et al. 2015). Most projections of future heat stress have neglected potential changes in shortwave and longwave surface radiation.

Given the ad hoc status of this menagerie of heat stress measures—which all weight temperature, humidity, wind speed, and radiation differently and have different conceptual and empirical bases—it is not obvious that patterns should exist that are robust across metrics or are accessible to theoretical understanding. We have studied behavior across a wide swath of metrics and find that the important variation can be condensed down to a few exemplars, spanning those metrics that place little weight on moisture and those that weight moisture heavily. Unfortunately, as in most other prior work, we do not have the scope to cover metrics that explicitly include wind speed or radiation as well. Despite all these limitations, some general behaviors emerge that can be useful for predicting future heat stress and the responses to it, as shown below.

2.3.1. Wet bulb temperature. One measure of heat stress proposed by Haldane (1905) that must be considered a fixed, upper boundary for a fit, acclimated individual drinking water freely in a strong breeze in the shade is wet bulb temperature, T_w. This quantity indicates the temperature that a maximally evaporatively cooled surface (such as sweaty skin) can approach. T_w is one of the three terms that make up WBGT (see Section 2.3.2). As is well known (Haldane 1905) and as further described in Sherwood & Huber (2010), physical labor becomes difficult to impossible when T_w exceeds 31°C, while exposure to T_w greater than 35°C for more than 6 hours leads to death even in fit, acclimated individuals. Sherwood & Huber (2010) used it as a first principles framework as a physical limit to human adaptive capabilities in heat stress. Their results show that if CO_2 injection into the atmosphere continues to grow for the next century, 50% of Earth's surface where people currently live will become uninhabitable at some point during an average year, barring the presence of strong heat mitigation procedures, e.g., air conditioning. This T_w threshold is fairly applicable to all placental mammals (Sherwood & Huber 2010) and cannot change with future acclimatization because it rests on biological constraints that only change,

at best, on evolutionary timescales. Recent work has increased awareness among the scientific community of T_w in quantifying the impacts of climate change on heat stress (Willett & Sherwood 2010, Fischer & Knutti 2012, Pal & Eltahir 2016). Our current climate's proximity to the danger threshold is particularly alarming given the possibility of major climate warming over the next century.

2.3.2. Wet bulb globe temperature and simplified wet bulb globe temperature. As previously mentioned, the WBGT was developed as a heat stress warning system for the US Marine Corps because of casualties during training in the 1950s (Minard et al. 1957). The metric uses a combination of wet and dry bulb temperatures as well as a globe thermometer, an instrument that measures an estimation of solar radiation. Since then, the metric was adopted for heat warnings in mines (Wyndham & Atkins 1968) and later as an international standard (Parsons 2006). There are numerous simplifications of WBGT [e.g., simplified WBGT (sWBGT)] geared toward avoiding using iterative methods of complex calculations for both wet bulb and globe thermometers (Hyatt et al. 2010, Willett & Sherwood 2010, Fischer et al. 2012). Relating WBGT to workplace heat stress, numerous studies evaluated potential changes in workers' labor capacity from a global change perspective (Baker et al. 2002, Kjellstrom & Mercado 2008, Kjellstrom et al. 2009b, Hyatt et al. 2010, Nilsson & Kjellstrom 2010). The first global assessment of heat stress and its impact on labor (Kjellstrom et al. 2009b) used global daily output of RH and temperature to calculate sWBGT. Although the study does not capture the diurnal cycle (losing the extremes of heat stress) and neglects the impacts of radiation, the authors are interested in long-term averaged future climate. sWBGT values are calculated from output using CO_2 concentrations from the A2 greenhouse gases scenario, and the study calculates a worker productive capacity based on sWBGT. The results show that some regions lose up to 25% of their labor capacity (e.g., Southeast Asia), and other regions lose up to 20% of their gross domestic product (e.g., Central America). These methods have been criticized for oversimplification and inaccuracies (Budd 2008), and advanced calculations for wet bulb and globe thermometers have been developed for the highest accuracy (Azer & Hsu 1977a,b; Davies-Jones 2008, 2009; Liljegren et al. 2008) (see **Supplemental Figure 1** for an example). These advanced calculations are now being used in simplified approximations for the more well-validated heat stress metrics, as described further below (Fischer & Knutti 2012, Fischer et al. 2012, Dunne et al. 2013). In a recent study on heat stress's impacts on total labor capacity (Dunne et al. 2013), the two major results from the study were (*a*) that by 2200 in the high CO_2 simulation, peak labor capacity during the warm season is less than 50% of the total potential labor capacity and (*b*) that the end of the twentieth century saw global labor capacity decrease by 10%. This is truly a disturbing result with profound societal consequences globally.

Supplemental Material >

2.3.3. Heat index. The National Weather Service (NWS) uses heat index (HI), a polynomial equation, for measuring apparent temperature (AT) (so-called feels-like temperature) and informs meteorologists when to issue excessive heat warnings (Steadman 1979, Rothfusz 1990). HI is calibrated for working conditions and used for determining labor working time and rest break frequency. HI shares many commonalities with the humidity index (humidex) and AT. These metrics all show the effect of moisture as a feels-like amplification of temperature. One of the first major modeling studies using metrics that included temperature and humidity focused on the Mediterranean (Diffenbaugh et al. 2007). The study used regional climate model output to calculate the HI, combining summer seasonal averaged RH with daily minimum and maximum temperatures to do so. Their high CO_2 scenario has three times more HI heat wave days as compared to their modern control. However, that study employed monthly means to calculate

HI, which can introduce systematic biases due to nonlinear turbulent, transient perturbations (Buzan et al. 2015) (see **Supplemental Figure 2** for an example).

Supplemental Material >

3. OVERVIEW OF MODERN HEAT STRESS REGIMES

The different heat stress metrics have been used, like different lenses, in **Figure 2** to identify fundamentally different patterns and drivers of heat stress. In terms of the temperature and humidity covariances (**Figure 2*e***) that produce extreme HI conditions (**Figure 2*c***), it is temperature extremes that dominate (**Figure 2*g***). Through the lens of T_w (**Figure 2*d***), moisture extremes dominate over much of Earth, with the exception of northern midlatitudes, where moisture and temperature extremes are equally important (**Figure 2*b***). sWBGT (**Figure 2*b***), unsurprisingly because of its construction, lies in-between (**Figure 2*f***), and the relative importance of temperature versus moisture extremes is a regional concern. The partitioning between temperature and moisture in each metric becomes more apparent when going from the seventy-fifth to the ninety-ninth percentile (see Buzan et al. 2015, figures 3–5). It is the moist metrics, T_w and sWBGT, that link most closely with survivability and labor capacity and that tend to be maximized in the regions with the highest population density (**Figure 2*a***). This is of special importance because these regions are most vulnerable to future increases in moist heat stress. This sort of statistical characterization lacks physical insight, so some brief description of relevant synoptic and large-scale atmospheric drivers is provided here.

3.1. Dry Versus Moist Heat

Much of the existing literature focuses on heat waves and heat stress defined as anomalous periods of high dry bulb temperature (Burke et al. 2015, Horton et al. 2015, Lauwaet et al. 2015, Weber et al. 2015, Yang et al. 2015, Ratnam et al. 2016). Anomalous periods of hot and dry conditions typically occur under prevailing high pressure conditions (e.g., blocking events or in subtropical subsiding regions). These conditions are typically hot and sunny, leading to exceedances of dry bulb temperature and shortwave radiation impact heat stress measures. This is often the case in arid to semiarid regions. A significant body of recent research demonstrates clear linkages among extreme summer temperatures, reductions in precipitation, prevalence of stable highs (i.e., blocking), and reductions in synoptic-scale eddy activity (Horton et al. 2015, Lehmann & Coumou 2015, Boschat et al. 2016, McKinnon et al. 2016). These anomalous circulations are potentially a remote response to distant sea surface temperature (SST) anomalies arising through the modulation of high-frequency waves by low-frequency planetary waves; the quasi-resonance of these waves is potentially important (Teng et al. 2013, 2016; Petoukhov et al. 2013, 2016; Coumou et al. 2014; Screen & Simmonds 2014). This is a powerful conceptual model that focuses more on temperature extremes than on humidity. These might be described as an explanation for dry heat waves and may provide key insights into the types of heat waves identified with HI.

One can contrast the dynamics between dry and moist heat scenarios. Typical dry heat scenarios involve high pressure systems with clear skies, allowing shortwave radiation to reach Earth's surface and causing hot (dry bulb) temperatures. In contrast, moist heat scenarios involve the convergence of moist air into low pressure systems, reducing the body's ability to evaporatively cool. When persistent low pressure conditions dominate and it is hot—and may be associated with relatively wet, cloudy, sometimes rainy conditions—measures of moist heat stress, related to T_w, including sWBGT can record very high values. These are situations with hot, wet, low-level thermodynamic environments that are often on the verge of moist convection (Russo et al. 2017, Im et al. 2018, Kang & Eltahir 2018, Sherwood 2018, Liu et al. 2019). Clearly, this dry versus wet

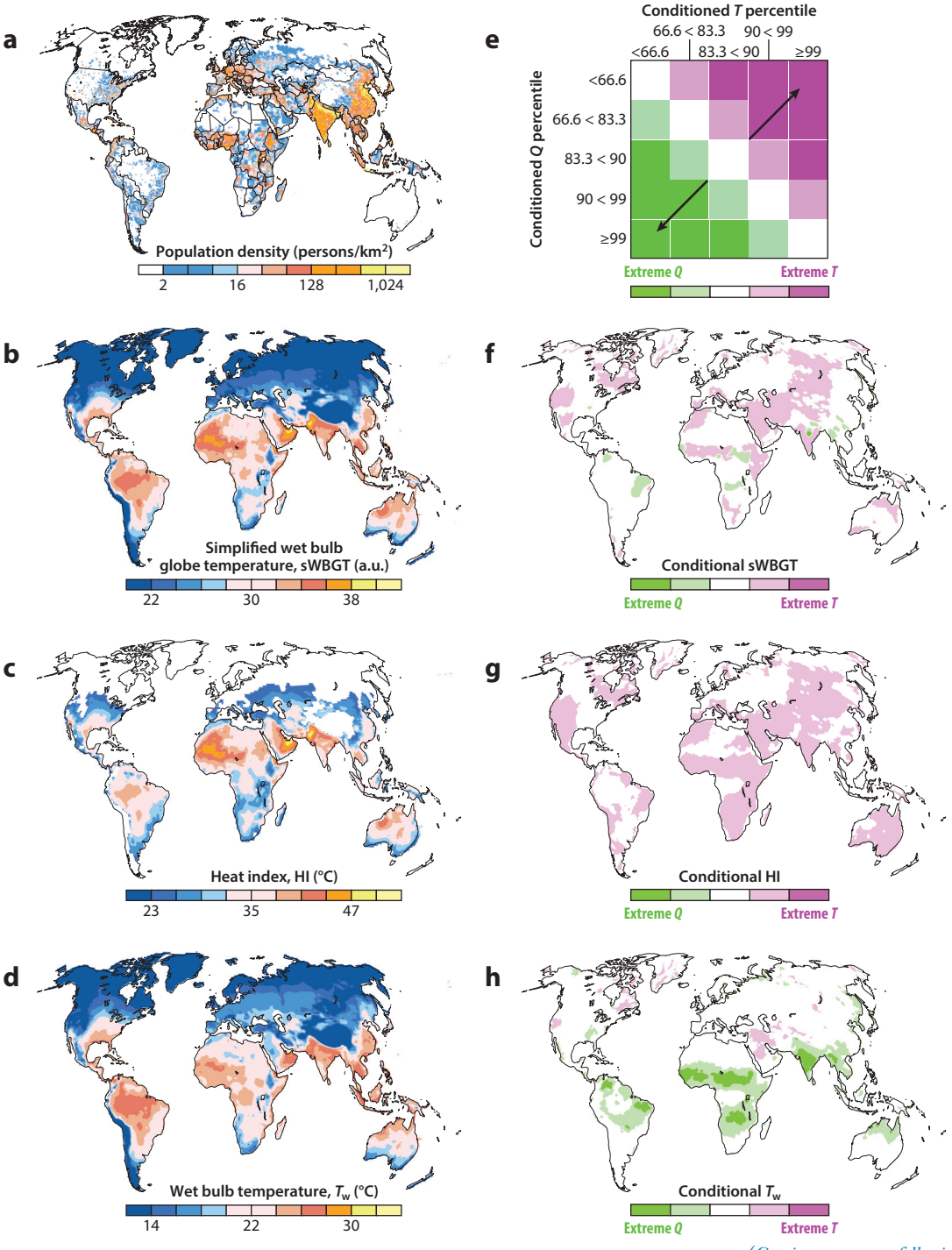

(*Caption appears on following page*)

Figure 2 (*Figure appears on preceding page*)

Maps showing 2010 population density, 1901–2010 CRUNCEP reanalysis maximum heat stress and relative contribution of $T-Q$, and a conditional $T-Q$ diagram, where T is temperature, T_w is wet bulb temperature, and Q is moisture: (*a*) population density, (*b*) sWBGT, (*c*) NWS HI, (*d*) T_w, (*e*) conditional $T-Q$ diagram, (*f*) conditional sWBGT, (*g*) conditional NWS HI, and (*h*) conditional T_w. Abbreviations: HI, heat index; NWS, National Weather Service; sWBGT, simplified wet bulb globe temperature. Figure adapted from Buzan et al. (2015).

dichotomy can break down under many circumstances—for example, when heat loads are driven equally by both terms, or when the dynamics of one are clearly related in space or time to the other. This can occur when a kinked jet stream generates a dry heat wave along the ridge and a moist heat wave in the trough. Given how well studied dry heat waves are, we do not focus on them in depth any further.

3.2. Future Moist Heat Extreme Projections

In this section we summarize the behavior of moist heat stress metrics in global circulation models for a late twentieth-century baseline and late twenty-first-century projections. We use output from 18 simulations from the Representative Concentration Pathway 8.5 (RCP8.5) Coupled Model Intercomparison Project Phase 5 (CMIP5) scenario (Taylor et al. 2012, Kobayashi et al. 2015). Simulation output at four times daily resolution (**Supplemental Table 1**) is used to calculate a multimodel mean (MMM) for the late twenty-first century (at an average 3.7°C of global warming; **Figure 3*a***) as compared to the late twentieth-century baseline MMM. Of course, the first step in using climate model output to project the future is validating the models, and the CMIP5 ensemble does remarkably well at reproducing the spatial pattern of multimetric heat stress observed in the Japanese 55-year Reanalysis (JRA55). The spatial variabilities in each metric from the late twentieth-century CMIP5 and JRA55 models are compared to each other, with pattern correlations of >0.95 (**Supplemental Table 2**). To give an idea of intermodel spread for modern conditions, the standard deviation (σ) between the CMIP5 models is 1.75°C in the late twentieth-century baseline except in the Andes Mountains, Sahel, Arabian Peninsula, and interior Asia (**Figure 3*b***).

Supplemental Material >

It is informative to begin by examining the behavior of T_w. At the end of the twenty-first century, the MMM shows substantial warming of T_w extremes (**Figure 3*a***). The hottest two weeks of an average year in India, eastern China, Southeast Asia, interior South America, and western Africa experience T_w >28°C. The intermodel standard deviation in the late twenty-first century shares many spatial features with the modern era (**Figure 3*c***), which suggests some robust intermodel biases. On top of that is a shift in standard deviation to higher values, which likely reflects the different global warming experienced by each model under RCP8.5 forcing. Closer inspection of a high transient climate response (TCR) CMIP5 model simulation (a 4.5°C global mean surface temperature change between 1986–2005 and 2081–2100) and a low TCR simulation (2.7°C; **Figure 4*a*,*b***) suggests this may be the case. In the high TCR case, changes in extreme T_w are homogenous except for the Sahel, Andes Mountains, Arabian Peninsula, Iran, and Pakistan (**Figure 4*a***). The low TCR case shows nearly uniform changes except for southwest Australia, a small section of the Sahel, and the Himalayan Mountains (**Figure 4*b***).

The starting point for this interpretation is that the shape of the probability density function for T_w is nearly invariant as climate changes, although the mean value shifts as a function of global mean temperature (Sherwood & Huber 2010; Pal & Eltahir 2016; Im et al. 2017, 2018). A simple understanding of how each heat stress metric changes as a function of the global mean surface temperature is expressed in terms of changes in the metric value per degree of globally

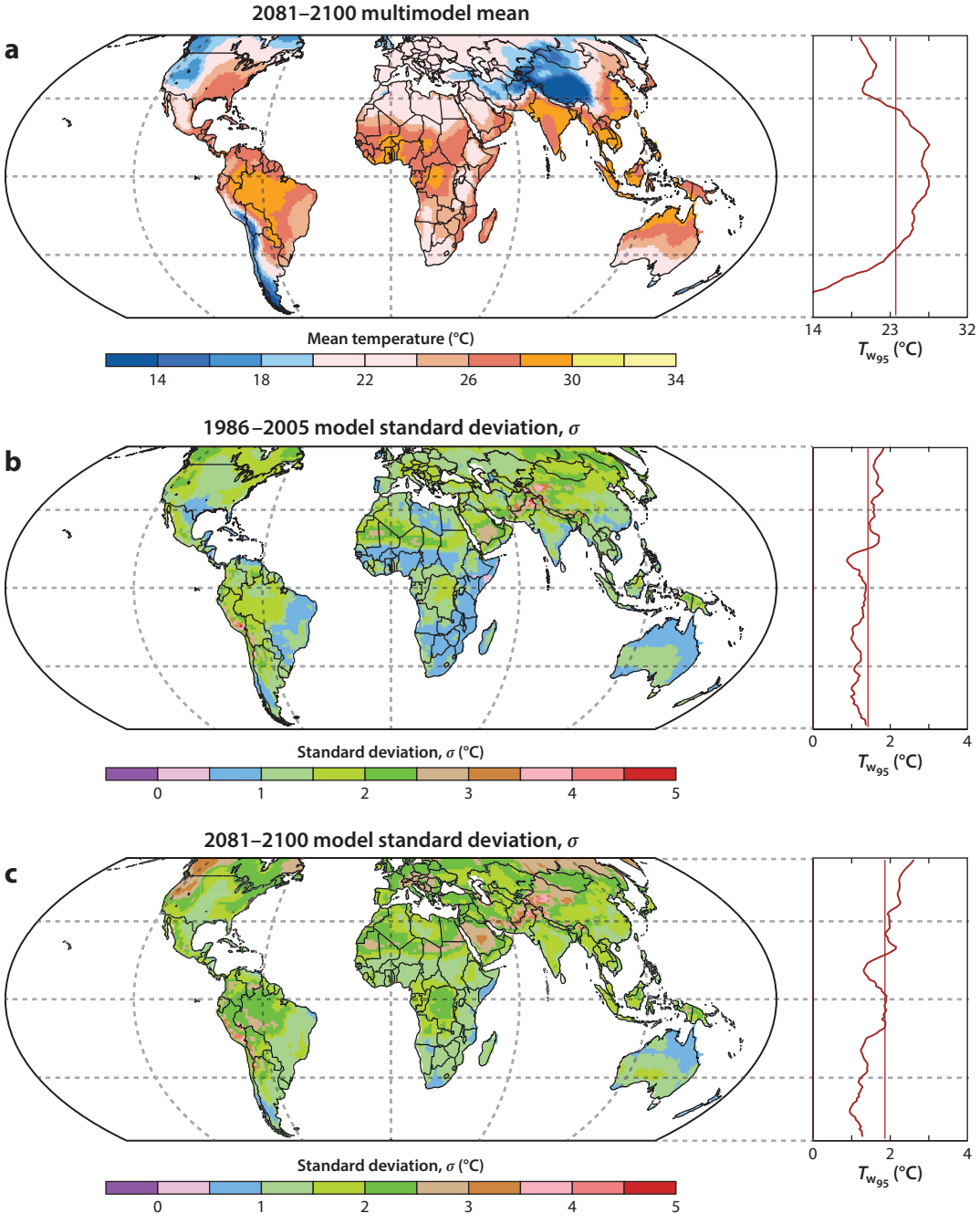

Figure 3

Maps and zonal means of T_w, the wet bulb temperature, characteristics in the CMIP5 archive: (*a*) late twenty-first-century (2081–2100) multimodel mean, (*b*) late twentieth-century model standard deviation (1986–2005), and (*c*) late twenty-first-century model standard deviation (2081–2100). Abbreviation: CMIP, Coupled Model Intercomparison Project.

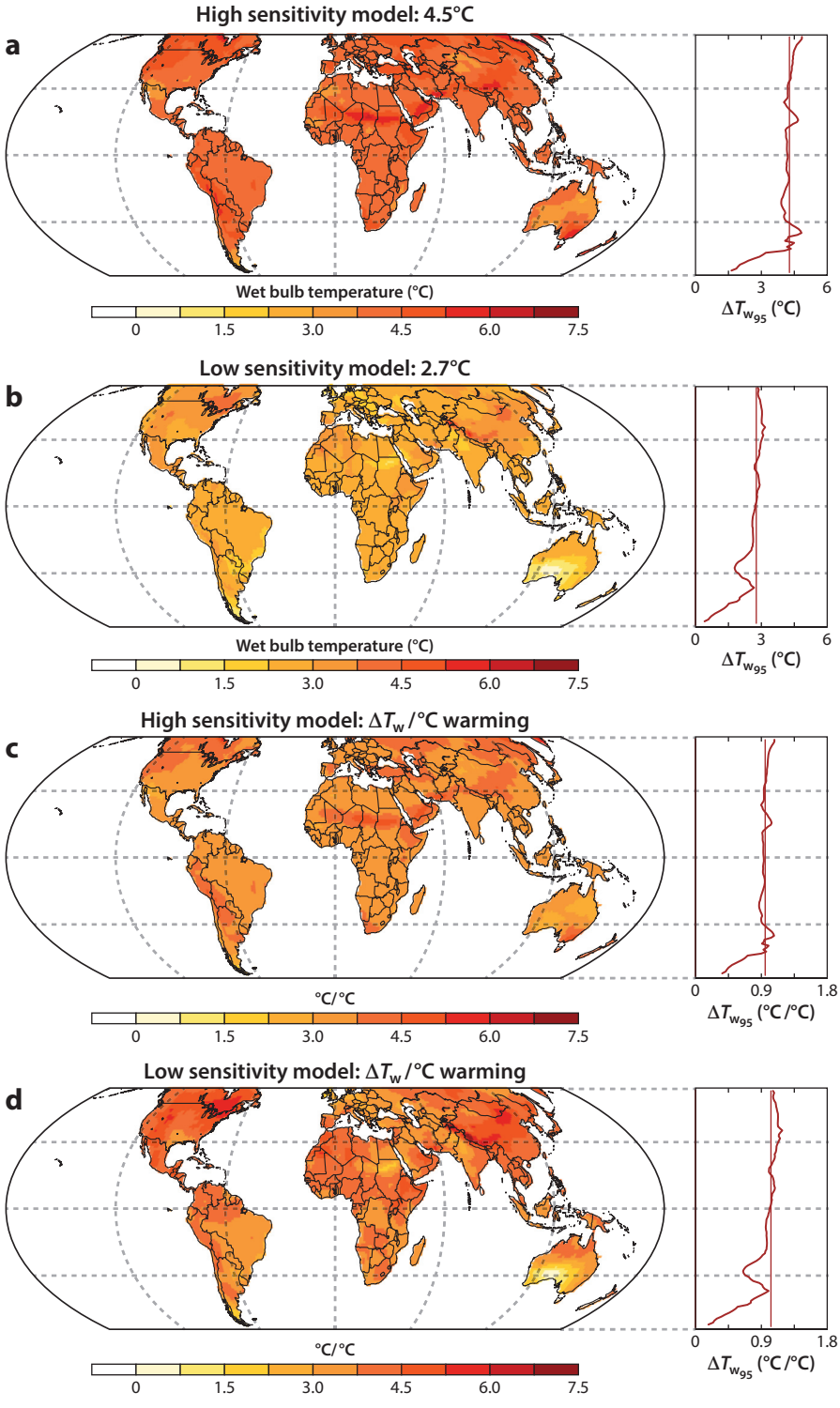

Figure 4

Maps of T_w, the wet bulb temperature, and zonal means of high (4.5°C) and low (2.7°C) sensitivity CMIP5 models: (*a*) ΔT_w of high sensitivity model, (*b*) ΔT_w of low sensitivity model, (*c*) ΔT_w per degree of warming (slope) of the high sensitivity model, and (*d*) ΔT_w per degree of warming (slope) of the low sensitivity model. Abbreviation: CMIP, Coupled Model Intercomparison Project.

averaged warming. This normalization removes TCR, which is closely related to equilibrium climate sensitivity—i.e., the different global mean temperature responses to the climate forcing in each model—from the problem. Dividing these changes by their respective global mean surface temperature changes produces the sensitivity of extreme T_w to global temperature change.

We can generalize this approach and define for any metric a sensitivity or slope parameter (Γ) as the change of each metric as a function of global mean surface temperature changes. In the formula below, X is the heat stress metric and 95 is the threshold percentile (extremes). Each metric in the formula is normalized by its respective globally averaged CMIP5 member temperature change, called the slope parameter:

$$\Gamma_{X,95} = \frac{\Delta X_{95}}{\langle \Delta T \rangle}, \qquad 1.$$

where $\langle \Delta T \rangle$ is the globally averaged temperature change and ΔX_{95} is the change of the metric in each grid cell. No heat stress metrics were designed to be applied to polar latitudes, so globally averaged $\langle \Gamma_{X,95} \rangle$ represents the subglobal averaged slope parameter (**Figure 5**) [subglobal (57°S to 57°N) and tropical (30°S to 30°N) slope parameter values are listed in **Supplemental Table 3**].

Supplemental Material >

For the high sensitivity case, excluding the Sahel, Arabian Peninsula, and southwestern North America, these slopes are nearly uniform, ~0.9–1.0°C/°C (**Figure 4*c***). However, at low sensitivity the slopes are nearly linear, ~0.9–1.1°C/°C, with high slopes in interior Asia, East Africa, and North America (**Figure 4*d***) and a low slope in southern Australia.

Expanding upon individual high and low sensitivities, how do these slopes apply to the entire distribution of simulations? To do this, each CMIP5 simulation ΔT_w between the late twenty-first and late twentieth centuries is divided by its respective global mean surface temperature changes. The MMM (**Figure 5*a***) and ensemble standard deviation (**Figure 5*b***) are evaluated. The MMM shows a high slope zone in the Sahel (1.1°C/°C), a low slope area in the southeastern United States (0.8°C/°C), and fairly uniform slopes 30°N southward (**Figure 5*a***). There are high slopes in the high latitudes (>1.2°C/°C). The standard deviation of these slopes is small and uniform (**Figure 5*b***), excluding the Sahel region. The scaling technique demonstrates that CMIP5 models have tightly bound moist thermodynamic behavior that is consistent across the archive and hints that there is a possible unifying theory for extreme moist heat stress.

4. A DEEPER DIVE INTO MOIST HEAT STRESS

4.1. Why Is Moist Heat Stress More Predictable than Dry?

As demonstrated above, T_w has muted and homogeneous responses to global mean surface changes. In fact, after scaling different climate models by their change in global mean surface temperature, maximum intermodel differences reduce to less than 1°C per 3.7°C of warming, which is remarkably robust compared to other dry metrics. At first glance this is confusing: Why would the statistics of the compound distribution of extreme value temperature and humidity be more predictable than one variable (temperature) alone? The next section explains why this is and why this means that moist heat stress is more robustly predictable than dry heat stress.

4.2. Thermodynamic Moist Heat Stress Framework

Consider the hottest, wettest, most unbearably muggy conditions you can imagine, such as the premonsoon season in India or just before an afternoon thunderstorm in August in the US

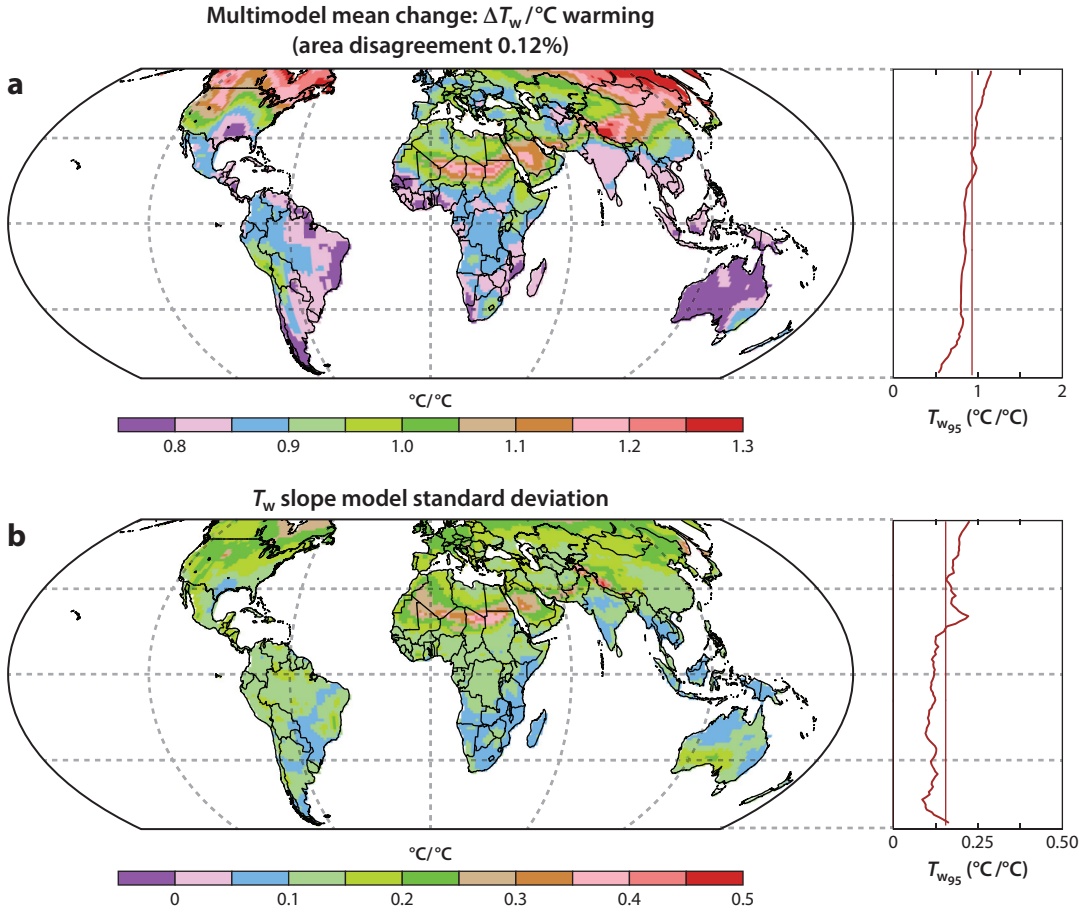

Figure 5

Maps and zonal means of scaling characteristics of T_w, the wet bulb temperature, in the CMIP5 archive. (*a*) Multimodel mean change in T_w per degree of warming (slope). (*b*) T_w slope model standard deviation. The area of disagreement in panel *a* is calculated by the coefficient of variation, $c_{v,\Gamma,X,95}$, >0.35 between CMIP5 simulations (area of disagreement is too small to see here). Abbreviation: CMIP, Coupled Model Intercomparison Project.

Midwest. Such conditions are clearly ones of high moist heat stress. These are also conditions on the threshold of convection, when an air parcel near the ground is buoyant (hot and wet) enough to ascend. Because of convective instability, a direct link exists between bulk thermodynamic properties of the troposphere and near-surface heat stress.

The atmosphere is observed to be in a state of convective quasi-neutrality (quasi-equilibrium) for much of the tropics (Emanuel 1995, Williams et al. 2009, Hoyos & Webster 2011) and into the midlatitudes during summer (Frierson 2006, Korty & Schneider 2007). Convective quasi-neutrality only becomes more prevalent with global warming (Zamora et al. 2016). For most landmasses in summer, atmospheric profiles are close to moist convective neutrality most of the time (**Figure 6**), and this condition is more nearly met precisely during high moist heat stress events.

In a warmer world, we expect changes in tropopause buoyancy, as identified by an increase in tropopause θ_{es}, to be of a similar magnitude to changes in the maximum θ_e near the surface (Wu & Pauluis 2014, 2015). But T_w is a close cousin of θ_e because they are both conserved

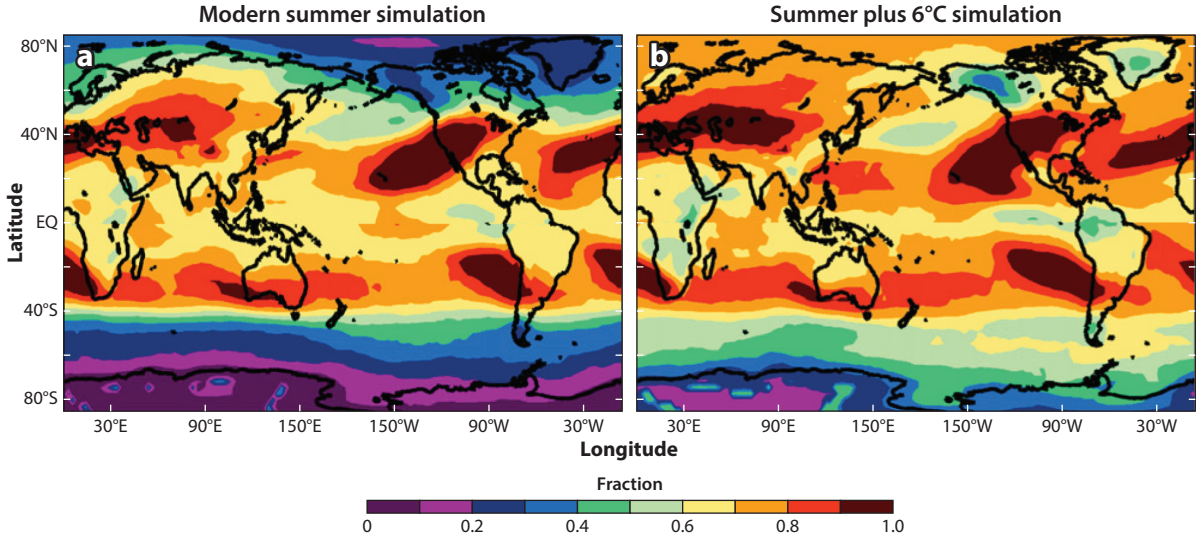

Figure 6

Fraction of summer that the atmosphere is close to moist adiabatic for two climate states: (*a*) modern and (*b*) about 6°C warmer. These simulations were carried out using the National Center for Atmospheric Research Community Climate System Model as described further in Zamora et al. (2016).

quantities under pseudoadiabatic ascent as shown in this simplified equation from equation 3.4 in Davies-Jones (2008):

$$T_w = 45.114 - 51.489\left(\frac{\theta_e}{C}\right)^{-\lambda}, \qquad 2.$$

where λ is the inverse of the Poisson's constant, $1/\kappa_d$, and $\kappa_d = R_d/c_{pd}$ (R_d is the dry air gas constant, and c_{pd} is the heat capacity of dry air at p).

The implication of this direct relationship is that moist heat stress extremes can be understood in terms of constraints imposed by moist convective neutrality (Sherwood & Huber 2010), i.e., that changes in near-surface θ_e are closely tied to tropopause θ_{es}. This limits the possible combinations of temperature (T), moisture (Q), and pressure (P) that can be expected at upper percentile levels for a given climate state. From this perspective, T_w strictly—and, to a lesser degree, any heat stress measure that approximates a thermodynamic variable (Fischer & Knutti 2012)—will be bounded for a given climate state by this convective constraint. This is complicated by the fact that, even in regions where moist heat stress is endemic, such as the tropical convecting and monsoonal regions, attempting to understand the climatological and synoptic drivers of moist heat stress immediately encounters the difficulties associated with complex and challenging circulations, including the drivers of the monsoon; the intertropical convergence zone; and transient, synoptic phenomena such as monsoon depressions (Hurley & Boos 2015). Nevertheless, the good news is that sound theories exist for moist, convective systems, from hurricanes to monsoons to Hadley circulations (Emanuel et al. 1994, Emanuel 1995), and these will provide a sound scaffolding for making robust projections for the future (Williams et al. 2009, Hoyos & Webster 2011, Zamora et al. 2016).

Convective constraint: moist hot air becomes convectively unstable and ascends; surface heat stress extremes link to these upper atmospheric dynamics and radiation

4.3. Minimal Moist Thermodynamic Model and Observations

With this grounding, a minimal model for all the heat stress metrics and their sensitivity to global climate change can be developed, calibrated with modern observations (JRA55 reanalysis), and

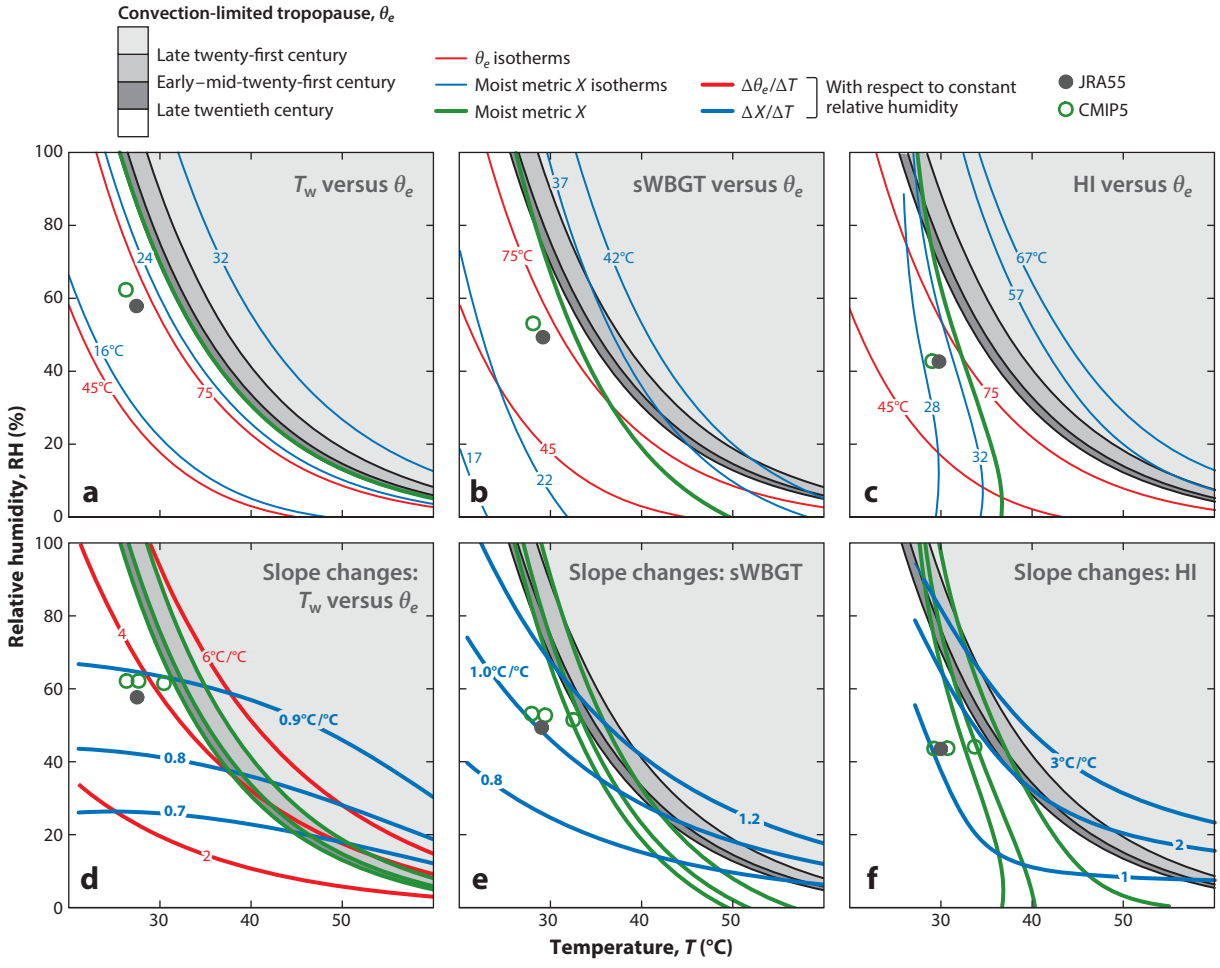

Figure 7

Moist thermodynamic state diagram where T is temperature, T_w is wet bulb temperature, and X is the heat stress metric. Convection-limited θ_e (*grays*) and moist metric X (*green lines*) are extracted from ninety-fifth-percentile spatial maximum CMIP5 ensemble climate states for the late twentieth century (1986–2005), early to mid-twenty-first century (2026–2045), and late twenty-first century (2081–2100). Average ninety-fifth-percentile temperature and RH are extracted from average ninety-fifth-percentile X (CMIP5, *green circles*; JRA55, *gray dots*). Abbreviations: CMIP, Coupled Model Intercomparison Project; HI, heat index; JRA55, Japanese 55-year Reanalysis; sWBGT, simplified wet bulb globe temperature.

compared with results from future projections from climate models. Our goal here is to derive basic scaling relationships between a given temperature change and the associated change in a variety of heat stress metrics. Although this framework applies more strictly within a single column of the atmosphere, we find that it adequately describes the bulk, average behavior of most of the atmosphere.

As a gross first approximation, imagine an Earthlike climate schematically represented in **Figure 7*a***. Tropopause θ_e is ~87°C, and the range of possible near-surface values is limited by moist convective equilibrium. Exceeding this limit implies ascent to the tropopause. Not all combinations of temperature and RH are possible for a given climate state—the range of possible values is much reduced. Thus, for a given climate state, maximum θ_e (therefore maximum T_w)

EXTREME HEAT AND FALSE THERMOSTATS

As summarized by Pierrehumbert (1995), Williams et al. (2009), and van Hooidonk & Huber (2009), theory, models, and paleoclimate data all demonstrate that warmer worlds have much warmer tropics than today. This is a crucial topic to consider when evaluating the ability of plants, animals, and ecosystems to adapt to hotter, more stressful conditions in the future. Although warming in the past (and presumably the future) is much amplified in high latitudes compared to the tropics, the tropics still warmed in past climates and provide the key constraint of being the highest θ_e/T_w temperature on the planet. For example, in the early Eocene, global mean temperatures were 15°C warmer and tropical temperatures 6–10°C warmer than modern (Huber 2008, Frieling et al. 2017, Cramwinckel et al. 2018). For a typical marine boundary layer relative humidity of 75%, such warm sea surface temperatures imply corresponding maximum surface T_w of 32°C. Thus, without any climate model results but solely considering basic physical limitations, we constrain heat stress even in the distant past. Mammalian thermodynamic limits should near the thermal limit over much of the tropics and subtropics.

Movable limit: with global warming the entire troposphere warms, thus moving the bounds on lower atmospheric buoyancy, and hence heat stress, to higher values

implies strong, broad constraint on combinations of temperature and RH. This limitation applies to all moist metrics (**Figure 7*b*,*c***): Roughly half the plausible range of Earthlike combinations of temperature and RH are disallowed, i.e., they would be convectively unstable, although the form of this constraint is sensitive to the details of heat stress metric formulation. This disallowed regime is not fixed (**Figure 7*a***) and shifts to hotter values with increasing global mean temperature since maximum θ_e increases, which we call a movable limit (see sidebar titled Extreme Heat and False Thermostats).

Using this same diagram (**Figure 7**) and the definitions of the various metrics and assuming a constant RH, it is straightforward to compute the derivatives of the metrics with respect to temperature. This diagram provides a simple minimal model for moist heat stress metrics, and the minimal model applies remarkably well to the detailed results from climate models. For example, we can immediately estimate that T_w should change by about 0.9°C per degree of warming knowing only the initial state. These derivatives are state dependent because of the underlying nonlinearity of the metrics themselves. As another example, any given isopleth $d\theta_e/dT_w$ is parallel to θ_e and T_w, but the change with respect to temperature (with RH constant) is strongly state dependent and nonlinear for θ_e (**Figure 7*d***); it can change by anywhere between 1.5 and 9°C per degree of warming, depending on the initial reference state assumed (**Supplemental Table 4**). T_w is nearly constant and linear. Typical fluctuations of θ_e and T_w are nearly identical at cold temperatures but differ by a factor of 10 at higher temperature values (see Davies-Jones 2008, equation 3.9). T_w changes by only 0.6–0.9°C per degree of warming over the same range of higher temperatures. sWBGT exhibits similar behaviors as T_w, with a near linear change in the metrics with respect to temperature (**Figure 7*e***). This logically follows, as T_w is a key component in the metric. HI exhibits nonlinear slope behavior with respect to temperature, although not to the same extent as θ_e (**Figure 7*f***). T_w is clearly well poised to be a metric that behaves very predictably as temperature changes.

Supplemental Material >

4.4. Comparison of the Minimal Model with Complex Models

This minimal model, including the derivatives of heat stress metrics, already provides a rough, but useful, approximate estimate of the response by more complex models in relation to global warming. To get more from this minimal model, in terms of realism, requires specifying the initial reference state because of the inherent nonlinearity of heat stress (**Supplemental Table 4**). For

this analysis, and without loss of generality, a modern heat wave is defined as the ninety-fifth percentile of each metric over land and is calculated with its associated temperature and RH from the JRA55 reanalysis product. Conditionally averaging over these events from the entire JRA55 (later CMIP5) four times daily output (**Supplemental Table 5**) yields the expected values of temperature and RH associated with heat waves. But, because each metric weights temperature and RH differently, the expected combination of temperature and RH for every metric varies (**Supplemental Table 4**).

Disallowed zone: maximum buoyancy limits prevent many extreme heat stress values; however, these buoyancy limits shift with climate state

In keeping with this simple approach, constant relative humidity is assumed. Theory suggests that this assumption may be roughly true for seasonal timescales (Byrne & O'Gorman 2013), but this theory does not extend to extreme events. Calibrating this to a modern global mean surface temperature, we can test the minimal model against the aggregated behavior of explicitly calculated metric changes from future climate simulations from the CMIP5 ensemble. Linearizing around the average modern state derived from JRA55 (**Figure 7**) and taking the slopes for each metric generates a minimal null model for how bulk behavior of heat stress extremes should change in the future.

Supplemental Material >

To evaluate the predictive capability of this null model, we calculate the spatial averages of each heat stress metric across CMIP5 ensemble members to derive extreme heat stress values from the late twentieth, mid-twenty-first, and late twenty-first centuries. The average properties of these metrics (**Figure 7**) encompass all the spatial-temporal inhomogeneity and nonlinearity of explicitly calculated MMMs. The average temperature and RH derived from the CMIP5 late twentieth-century extremes for each metric are nearly identical to those predicted by the minimal null model, which is based only on the modern state and analytically derived derivatives (**Figure 7*a–c***).

Furthermore, the expected values of temperature and RH in the CMIP5 models are below the disallowed zone, demonstrating that all heat stress metrics are bounded by the convection limit on θ_e. Here, the disallowed zone is defined as the convection limit for a given climate state (i.e., a given global mean surface temperature) and is calculated as the $\theta_{e,95}$ corresponding to the top 5% of terrestrial spatial average for CMIP5 from all three time periods (**Figure 7**). As a further test, the top 5% of terrestrial spatial average calculation for $T_{w,95}$, sWBGT_{95}, and HI_{95} is used (**Figure 7**). These hottest values show that convective limit violations are rare and that temperature and RH combinations are typically even more restricted than possible by convective limits. Comparing the late twentieth- and end of twenty-first-century simulations (2091–1996) reveals that the CMIP5 ensemble progressively becomes drier with climate change for each metric (**Figure 7*d*,*e***). However, future extreme HI_{95} events are associated with higher relative humidity conditions, which makes HI_{95} an outlier compared to the other metrics (**Figure 7*f***).

4.5. Predicting Bulk Changes in Heat Stress Metrics from Thermodynamic Considerations

It is interesting to see if this simple theory for how these metrics change with temperature applies when compared with the spatial average of the full CMIP5 ensemble. One can start assuming a global constant RH value and a specified global mean surface temperature change in the simple model to see how it compares with the spatially averaged responses of the CMIP5 ensemble.

We compare the predictions of the relationships shown in **Figure 7** to the spatially averaged values of the slope parameter for each metric in **Figure 8**. Specifically, the average temperature and RH from JRA55 heat stress metric extremes were chosen and plotted. In addition, the CMIP5 historical periods (**Figure 8**) are plotted and have nearly identical slopes as JRA55 (**Figure 8**) with fixed RH. As revealed by the spindle diagrams showing CMIP5 slope parameters calculated

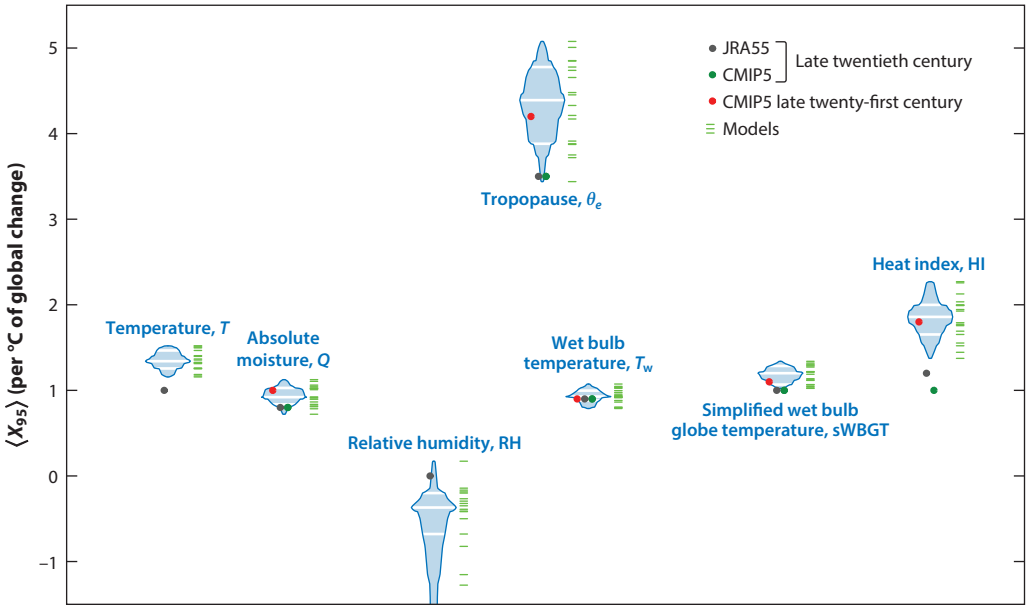

Figure 8

Intermodel spread 2091–1996 global mean ninety-fifth-percentile slopes (calculated over 57°S to 57°N). The spindle diagram contains the 18 CMIP5 simulations (width indicates concentration), with each individual model denoted by a horizontal green bar. The lower (*lower white bar*), median (*middle white bar*), and upper (*upper white bar*) quartiles represent 50% of the CMIP5 simulations; the tails are maximum and minimum, i.e., the range. The ninety-fifth-percentile slopes are late twentieth-century JRA55 (*gray*) and CMIP5 (*green*) and late twenty-first-century CMIP5 (*red*). Abbreviations: CMIP, Coupled Model Intercomparison Project; JRA55, Japanese 55-year Reanalysis.

between the late twentieth and late twenty-first centuries, the bulk behavior of heat stress is well predicted from the minimal theory, the exception being HI_{95}. The fixed RH assumption does well for most metrics projected to the end of the twenty-first century (**Figure 8**), with exceptions for $\theta_{e,95}$ and HI_{95}.

It has been proposed that slightly lower average RH is expected in future climates (Byrne & O'Gorman 2013, 2016), which is reflected in **Figure 8**; here, T_{95} has a median slope of 1.3, and RH_{95} is −0.3, resulting in 0.3% drying per degree of warming. Relaxing the constant RH assumption and instead using the ensemble mean CMIP5 derived change in RH brings the spatially averaged metric values directly computed from four times daily values in the CMIP5 ensemble into better agreement with the simple moist theory presented above (**Figure 8**). This drying effect is strongly expressed in HI_{95} and $\theta_{e,95}$ (**Figure 8**) and minimally seen in $sWBGT_{95}$ and Q_{95}. Because changes in $T_{w,95}$ behave linearly with changes in $\theta_{e,95}$, the effects of changes in humidity are minimal. In all metrics, the changes in the CMIP5 ensemble fall within the expected value of the late twenty-first century (**Figure 8**).

To summarize, this minimal model, which relies on nothing more than the equations that define the metrics and minimal assumptions for a global mean temperature and relative humidity, provides a solid framework for understanding and predicting the bulk response of heat stress extremes from more sophisticated CMIP5 models. To estimate the global average change in an extreme heat wave metric, a sophisticated climate model is unnecessary. The sophisticated models are, of course, necessary for predicting the spatially resolved patterns of change.

5. SCALED MULTIMETRIC, MANY MODEL HEAT STRESS PROJECTIONS

As a consequence of the robust behavior captured by the minimal model, the main value of CMIP5 simulations is predicting changes in the spatial dimension. A way to evaluate the spatial distributions of $\Gamma_{X,95}$ is through a pattern scaling (**Figure 9**). Pattern scaling temperature and precipitation with global mean surface temperature changes is a widely applied analysis (Seneviratne et al. 2012, Sillmann et al. 2013, Donat et al. 2017). Remarkably, the patterns of the slope parameter for each metric are nearly stationary. Pattern correlations of >0.93 between the CMIP5 ensemble $\Gamma_{X,95}$ are nearly constant, whether they are calculated from 2036 to 1996 or 2091 to 1996. Additionally, the coefficient of variation in each heat stress metric as compared to T_{95} is below the threshold value 0.35, defined as robust in prior work (Seneviratne et al. 2012). Having demonstrated that the models themselves currently predict heat stress suitably and that the bulk, spatially averaged behavior is well predicted by simple theory (**Figure 8**), the changes going into the future are robust in a multimodel sense and nearly stationary in time. Therefore, a detailed analysis of the resulting patterns is warranted.

5.1. Hotspots

Pattern analysis specifically emphasizes hotspots (Donat et al. 2017). In this analysis hotspots are defined as values that exceed the upper quartile of each metric in **Figure 8**. This draws attention to where the fixed RH assumption is a poor guide. Dry hotspots ($\Gamma_{T,95} > 1.5$) show up in the northern latitudes of North America, the interior of South America, and southern Africa (**Figure 9*a***; see **Supplemental Figure 3**). The CMIP5 model land area of disagreement is low (0.8%), and these hotspots are consistent with the analysis of dry heat waves (Sillmann et al. 2013).

Supplemental Material >

Dry and moist hotspots exist in the Mediterranean Sea region. A $\Gamma_{T,95}$ hotspot surrounds the Mediterranean Sea, i.e., western North Africa, the Middle East, Europe, and interior Asia. Although not covering the same spatial extent as $\Gamma_{T,95}$, the immediate area surrounding the Mediterranean Sea shows a coastal $\Gamma_{\mathrm{HI},95}$ maximum (**Figure 9*b***). $\Gamma_{\mathrm{sWBGT},95}$ has a hotspot over the Mediterranean Sea. Unlike $\Gamma_{\mathrm{HI},95}$, the hotspot extends into the Middle East (**Figure 9*d***).

Otherwise, each moist metric highlights hotspots that differ from $\Gamma_{T,95}$. $\Gamma_{\mathrm{HI},95}$ has a prominent hotspot (>2.0) in western and central Africa (**Figure 9*b***), which is the opposite of $\Gamma_{T,95}$. Furthermore, $\Gamma_{\mathrm{HI},95}$ in the eastern United States has a prominent hotspot east of the Rocky Mountains that extends down into the Caribbean and Latin America. Like the United States, China has a hotspot that is east of the Himalayan Plateau. South Asia, Southeast Asia, and northern Australia additionally share a hotspot. $\Gamma_{\mathrm{HI},95}$ has the highest model disagreement (19.7%), but this may be how the metric is constructed, as colder temperature CMIP5 variability transitions to the lower bounds of HI. $\Gamma_{T_{\mathrm{w}},95}$ is a fairly smooth field globally, with some notable exceptions, such as the hotspots of >1.05 at higher latitudes (**Figure 9*c***). There the Sahel shows a hotspot, as does the Himalayan Plateau. There is model disagreement in these locations, although overall disagreement is 0.1%. Additionally, $\Gamma_{T_{\mathrm{w}},95}$ shows the warming hole, previously noted in Rogers (2013), over the southern United States (<0.80). $\Gamma_{\mathrm{sWBGT},95}$ hotspots (>1.30) are in the high latitudes of North America and Asia, eastern China, central South America, and the Sahel (**Figure 9*d***). Otherwise, $\Gamma_{\mathrm{sWBGT},95}$ exhibits nearly uniform zonal behavior from 30°N to 30°S.

The hotspot comparison above highlights the importance of using multiple metrics to capture the diversity of potential impacts. Each metric is calibrated for specific weather or work conditions, and each is used operationally on a local or regional basis (Masterson & Richardson 1979, Epstein & Moran 2006). The disparity in their metric spatial slope parameter patterns shows that although the underlying moist thermodynamic theory is the same (**Figures 7** and **8**), they produce different

Figure 9

Maps and zonal means of multimodel mean extreme slope parameters: (*a*) $\Gamma_{T,95}$, (*b*) $\Gamma_{\mathrm{HI},95}$, (*c*) $\Gamma_{T_w,95}$ (repeated here from **Figure 5*a*** for comparison), and (*d*) $\Gamma_{\mathrm{sWBGT},95}$. The area of disagreement is calculated by the coefficient of variation, $c_{v,\Gamma,X,95}$, >0.35 between CMIP5 simulations (visually represented by *white stipple* in panels *a* and *b*; area of disagreement is too small to see here for panels *c* and *d*). Abbreviation: CMIP, Coupled Model Intercomparison Project.

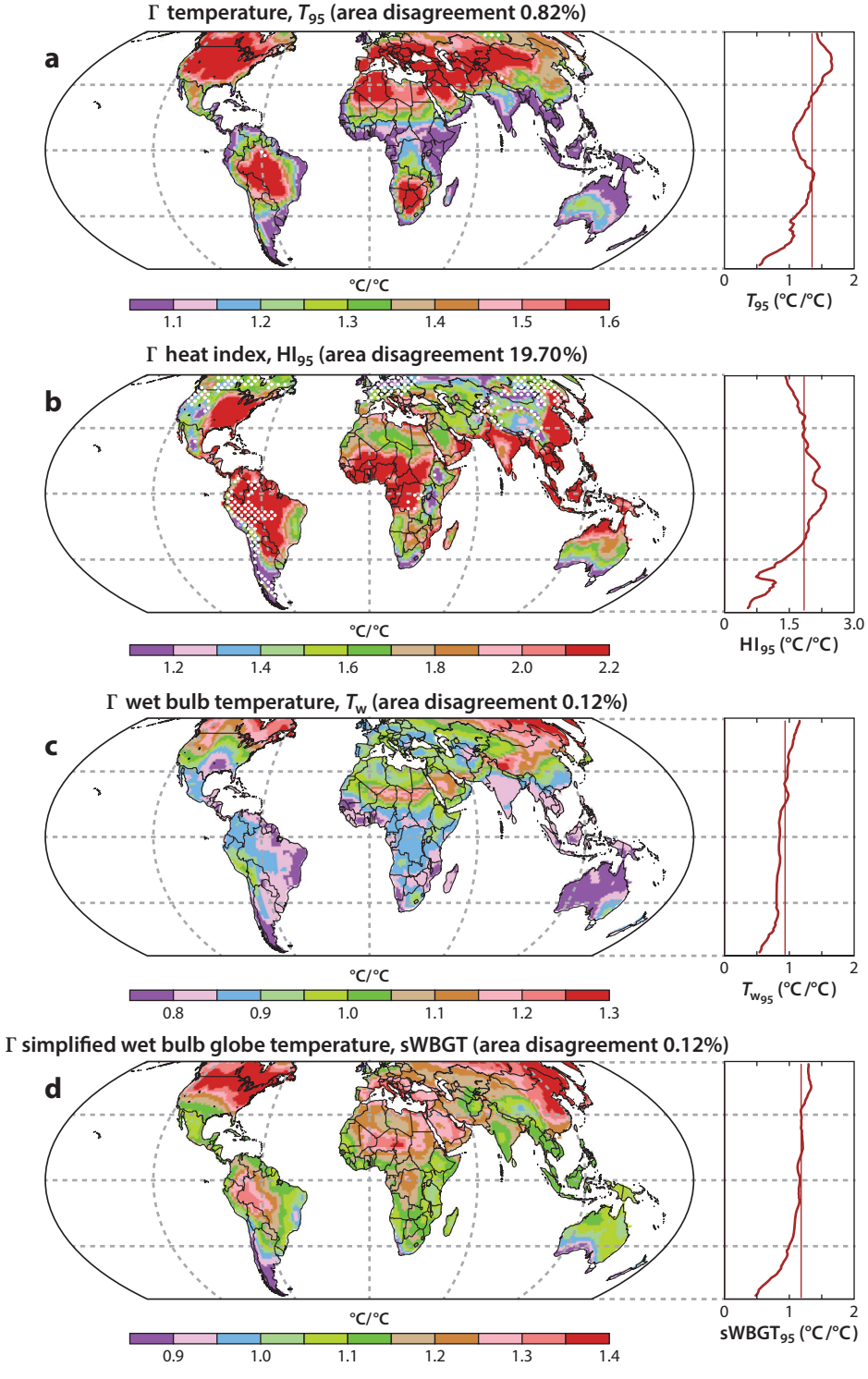

regional results (**Figure 9**). A strongly theoretically grounded prediction of future climate heat stress is possible using the globally averaged slopes. However, to capture the details of climate change requires using pattern scaling, which captures regional differences, and multiple metrics, which reveal pattern differences.

Within the myriad details produced by these different metrics, some order can be discerned. As described above, dynamic constraints on θ_e—buoyancy measures—and radiative convective principles place constraints on moist heat stress patterns (Emanuel 1995, Williams et al. 2009, Zamora et al. 2016). For metrics that weight T_w heavily (e.g., sWBGT), these patterns will closely resemble changes to the global mean sea surface temperature, as seen in recent theories (Williams et al. 2009, Hoyos & Webster 2011, Fischer & Knutti 2012, Korty et al. 2017) and observations (Williams & Pierrehumbert 2017). These T_w scaling relationships (**Figures 7*d*** and **8**) explain the nearly invariant behavior shown in recent studies using T_w (Pal & Eltahir 2016; Im et al. 2017, 2018). When global temperatures increase by ~7°C from today's global temperatures, the 35°C T_w threshold is crossed globally. Below, we discuss metric by metric the implications of these theories and how they fit within the broader topic of global heat stress.

South Asia has some of the highest T_w values in the world, with a broad area extending from the Indus Valley in Pakistan along northern India to Bangladesh, where T_w regularly exceeds 28–29°C (**Figure 2*d***). This same region has some of the world's highest population densities, containing roughly half a billion people (**Figure 2*a***). As a result, South Asia is a hotspot for heat stress risk, with a large population living very close to the threshold for degraded work capacity and the ultimate limit for survivability. The reality of this threshold is evidenced by the fact that in recent summers, thousands of people and tens of millions of livestock have died in unprecedented heat waves. Proximity to the danger threshold is particularly alarming given the possibility of major climate warming over the next century; events exceeding the 35°C threshold have already occurred in other high T_w regions, such as the Persian Gulf (Schär 2015), and such events are projected to become common there by the end of this century in a high-end warming scenario (Pal & Eltahir 2016; Im et al. 2017, 2018).

The $\Gamma_{T,95}$ spatial patterns mentioned before (**Figure 9*a***) agree with previous results of extreme temperature for the western Sahara Desert, southern Europe, interior southern Africa, interior South America, and interior Asia (Donat et al. 2017); North America and eastern China hotspots are similar to those identified in previous studies (Diffenbaugh & Giorgi 2012, Sillmann et al. 2013, Donat et al. 2017). But these patterns do not apply to all situations regarding heat stress. For example, extreme HI moistens with climate change (**Figure 7*f***), and each metric samples a different combination of extreme T–Q covariance (**Figure 7** and **Supplemental Table 5**).

Supplemental Material >

However, the pattern Diffenbaugh et al. (2007) found in the Mediterranean is retained in this analysis using $\Gamma_{HI,95}$ (**Figure 9*b***). HI correlates well with increased morbidity rates from heat waves that disproportionately affect the unfit, elderly, and infirm (Monteiro et al. 2013), and the results in **Figure 9*b*** highlight hotspot areas likely to be impacted. These scaling patterns are similar to a new metric on morbidity (Mora et al. 2017b), demonstrating that hotspots can highlight future areas impacted by heat-driven morbidity. Some caution is in order when interpreting these results, as HI is more variable between CMIP5 models than other metrics in midlatitudes.

Not all heat stress metrics, however, are entirely consistent with previous studies. The scaling $\Gamma_{sWBGT,95}$ (**Figure 9*d***) highlights hotspots in the Middle East, Northeast North America, and Northeast Asia not found in previous work by Zhao et al. (2015); their methods add 3°C without constraining the changes with climate models (Hyatt et al. 2010), or they compare modern observations with future climate simulations directly (Kjellstrom et al. 2013). To limit these inconsistencies, the community is encouraged to expand its use of multiple heat stress metrics to further identify and analyze key hotspots.

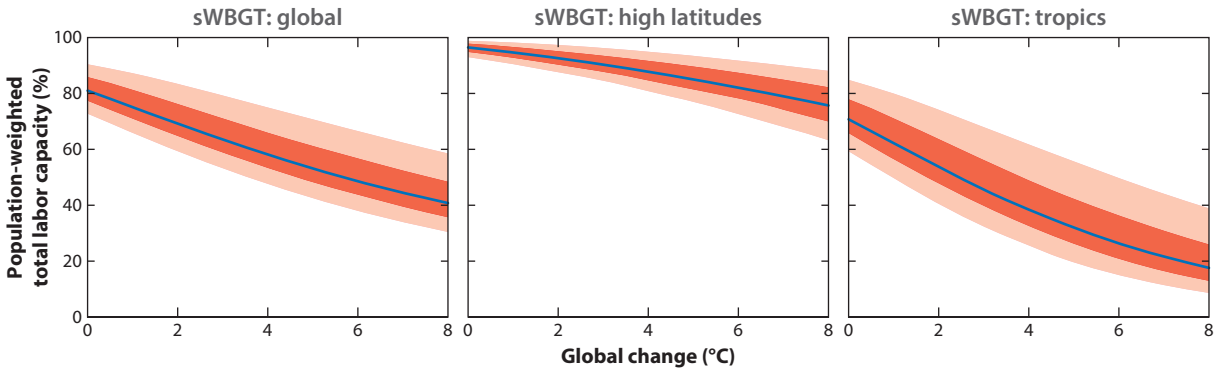

Figure 10

Population-weighted total labor capacity. The CMIP5 ensemble is represented by the median (*blue line*), 50% (*red swath*), and 80% (*pink swath*) confidence intervals. The relative impacts on labor are shown at global (57°S to 57°N), high latitude (outside of 30°S to 30°N), and tropic (30°S to 30°N) regions. Abbreviations: CMIP, Coupled Model Intercomparison Project; sWBGT, simplified wet bulb globe temperature.

5.2. Application to Future Labor Capacity

Besides morbidity and mortality, there are other heat stress impacts of concern from climate change, such as human labor damages. The slope parameters shown above are amenable to inclusion in simpler models, such as integrated assessment models (Burke et al. 2015, Fyke & Matthews 2015). For example, sWBGT can be condensed down to a capacity function, giving productivity as a percentage of total capacity per work hour (Dunne et al. 2013):

$$L_{\text{cap}} = 100 - 25\max\left(0, \text{sWBGT} - 25\right)^{\frac{2}{3}}, \qquad 3.$$

Supplemental Material >

where L_{cap} is on a scale of 0–100%. By using the stationarity Γ_{sWBGT} (**Supplemental Table 2**) and the late twentieth century as a baseline, as well as by assuming unchanging relative population densities, we show the population's weighted L_{cap} per degree of warming (**Figure 10**). The late twentieth-century baseline shows global losses to L_{cap} (80% total capacity), which is consistent with previous results (Hyatt et al. 2010, Dunne et al. 2013, Kjellstrom et al. 2013). The high latitudes show ~96% L_{cap} at the baseline, and the tropics median L_{cap} is ~71%. As previous models and studies show, climate change disproportionately impacts labor productivity in the tropics compared to the rest of the world. This vulnerability is due to a twofold phenomenon: First, the tropics have the highest labor heat stress conditions (**Figure 2*b***), and second, the highest population densities are in the tropics. At 4°C of warming, median L_{cap} in the tropics is at ~40%, while the high latitudes are at ~88%. Global capacity is at ~59%, reinforcing the claim that today's population labor distribution is vulnerable to future heat stress.

6. SUMMARY AND OPEN QUESTIONS

In the same way that heat stress at the individual level can reduce health and functional capabilities, widespread heat stress will have systemic negative impacts on societies and ecosystems, both managed and unmanaged. Heat stress mitigation and adaptation can place large and differentiated loads on energy and water production, as well as distribution infrastructure. These impacts have profound implications for the design of future food, energy, and water systems, in addition to economics, policy, governance, and equity considerations. Livestock and other mammals will

EVOLUTIONARY IMPLICATIONS OF HIGH HEAT STRESS IN THE PAST

The tropical and subtropical mammalian fossil record from past warm climates is sparse. This might be the consequence of the challenges of collecting fossils in most modern tropical locations, as well as tropical taphonomic biases. But records of mammalian diversity and size do exist in the midlatitudes. These records show profound and robust increases in the mass of major mammalian taxa from the early Eocene toward the present. The major taxa heavier than 1 kg—carnivora, artiodactyls, and perissodactyls—were all about a factor of 10 less massive during the early Eocene than subsequent periods (Alroy et al. 2000, Smith et al. 2004). Trends in heat stress, driven by the climatic cooling from the early Eocene, may provide a partial explanation for the apparent trend in mammalian body mass toward larger values (Cope's law) through the Cenozoic (Alroy 1998). Further evidence that this phenomenon might have been important is provided by the transient dwarfing of mammals in North America during the brief warming event at the beginning of the Eocene, known as the Paleocene–Eocene Thermal Maximum (Gingerich 2006), and in subsequent early Eocene hyperthermals (D'Ambrosia et al. 2017), which may have been an adaptation to enhance heat dissipation. Crucially, some of the evolutionary innovations that were required in these past high heat stress climates may reside within the genetic legacy of living organisms. However, much may have been lost in the grand Cenozoic cooling that led to bipolar glaciation.

continue to move indoors, and air conditioning for humans and livestock will increase energy demands. Besides humans, endotherms in general exhibit common biological susceptibilities and strategies for reducing their vulnerability to hot conditions. Thus, there are deep physical and biological commonalities existing between individual organisms, ecosystems, and human systems (see sidebar titled Evolutionary Implications of High Heat Stress in the Past). Recognizing the underlying similarities between rules that govern these different scales provides fundamental constraints on global systems as they change in the future.

SUMMARY POINTS

1. As long as humans can sweat, they can typically withstand extreme dry bulb temperatures. Consequently, heat stress from dry heat waves can be ameliorated by increased water availability. Common solutions for dealing with dry heat stress, such as sweating, swamp coolers, and green roofs, are primarily water resource problems.
2. In a warmer world, moist heat stress may occur over large regions for months at a time, including densely populated regions. In this so-called steambath world, dry solutions do not help even in the mean state and could even be lethal. This is different than dry heat stress, which tends to come in discrete heat waves associated with specific synoptic settings or climatologically in deserts where population densities are low.
3. Moist heat stress has special thermodynamic and dynamical constraints associated with moist convective equilibrium, making it uniquely predictable in a climatological sense. Consequently, moist heat stress distributions are robust and less model dependent than other projected variables, and they can be derived from other robust theoretical models for temperature and humidity variations. These scaling relationships constrain the limits of planetary habitability (Sherwood & Huber 2010, Goldblatt et al. 2013).
4. Scaling approaches derived from climate model output enable identification of regions that are especially susceptible to change, i.e., hotspots. These hotspots are different

between metrics; it is too early to reduce the number of metrics considered in impact studies, but qualitatively, metrics fall into two classes: linear change with respect to temperature (**Figure 7*d*,*e***) or nonlinear changes (**Figure 7*d*,*f***).

5. The tropics, which already suffer from high heat stress summers today (Matthews et al. 2017), will become permanently stressful year round (Fischer & Knutti 2012, Li et al. 2018), even with small changes in the average global temperature change (>2°C).
6. Heat stress ultimately threatens humans' capacity to perform work (Dunne et al. 2013, Kelley et al. 2015, Pal & Eltahir 2016, Im et al. 2017) and may reach deadly levels (Sherwood & Huber 2010, Pal & Eltahir 2016). For a given global mean surface temperature change, we can determine the limit of habitability for mammals; the main uncertainties are in the amount of climate change and not other details of modeled physics.

FUTURE ISSUES

1. Next-generation climate models need to resolve fine scales. The current generation of climate models typically used for both global and regional future climate change projection studies does not explicitly represent moist convection, so the key process that can cause or ventilate severe moist heat stress events is crudely parameterized. The parameterizations only roughly treat—or completely neglect—key processes such as convective inhibition and mesoscale convective organization. Future heat stress research must either develop a better and generalizable theoretical understanding of the cascade of interactions from large scale to fine, on convecting systems and their organization with regards to moist heat waves, or explicitly model these interactions using fine (sub-4-km) resolution weather models (e.g., Komurcu et al. 2018).
2. Global circulation models need to include land-use change. Land-use, irrigation, and associated evapotranspirative fluxes play a significant role in moderating dry heat stress in regions such as the warming hole in the United States (Alter et al. 2015, Lu & Kueppers 2015) and India (Kumar et al. 2017), but moist heat stress may be more complicated.
3. Global studies on heat stress need to include explicit wind and radiation calculations. Radiation is a critical component of heat stress (Brunt 1943, Minard et al. 1957) and was only recently included in regional modeling studies (Kasai et al. 2017). Many global studies using wet bulb globe temperature, however, omit the radiative component from heat stress, ignoring an important source of heat load on humans and animals (e.g., Smith et al. 2016).
4. The accurate, physiologically constrained, and physically robust metrics discussed here have normalized spatial patterns that are linear and bounded, and so are amenable to inclusion in simpler models, such as integrated assessment models and economic damage models (Burke et al. 2015, Fyke & Matthews 2015). Using such approaches, we can predict economic losses by using scaling techniques (Burke et al. 2015, Moore et al. 2017). We have demonstrated that a scaling approach can be used as input for a damage function in economic modeling with moist heat stress metrics (**Figure 10**), but such a function behaves nonlinearly.

5. Better prognostic and mechanistic models, representing human physiology, need to be incorporated and diagnostic metrics abandoned altogether.

DISCLOSURE STATEMENT

The authors are not aware of any affiliations, memberships, funding, or financial holdings that might be perceived as affecting the objectivity of this review.

ACKNOWLEDGMENTS

J.R.B. thanks B. Claytor for enhancing manuscript clarity. Computing resources support comes from the Swiss National Supercomputing Centre (CSCS) under project ID s906. M.H. thanks R. Caballero, K. Emanuel, and S. Sherwood for improving his thinking on heat stress. Computing resources from Information Technology at Purdue University were used in this research. We acknowledge the WCRP WGCM, which is responsible for CMIP, and we thank the climate modeling groups for producing and making available their model output. This review was supported by the NSF EPS 1101245 and CBET 1805808 awards to M.H. and by Purdue University's Discovery Park Big Ideas Challenge.

LITERATURE CITED

Alroy J. 1998. Cope's rule and the dynamics of body mass evolution in North American fossil mammals. *Science* 280:731–34

Alroy J, Koch PL, Zachos JC. 2000. Global climate change and North American mammalian evolution. *Paleobiology* 26:259–88

Alter RE, Im ES, Eltahir EAB. 2015. Rainfall consistently enhanced around the Gezira Scheme in East Africa due to irrigation. *Nat. Geosci.* 8:763–67

Azer N, Hsu S. 1977a. OSHA heat stress standards and the WBGT index. *ASHRAE Trans.* 83:30–40

Azer N, Hsu S. 1977b. The prediction of thermal sensation from a simple model of human physiological regulatory response. *ASHRAE Trans.* 83:88–102

Baker LA, Brazel AJ, Selover N, Martin C, McIntyre N, et al. 2002. Urbanization and warming of Phoenix (Arizona, USA): impacts, feedbacks and mitigation. *Urban Ecosyst.* 6:183–203

Barriopedro D, Fischer EM, Luterbacher J, Trigo RM, Garcia-Herrera R. 2011. The hot summer of 2010: redrawing the temperature record map of Europe. *Science* 332:220–24

Basu R. 2009. High ambient temperature and mortality: a review of epidemiologic studies from 2001 to 2008. *Environ. Health* 8:40

Bedford T, Warner CG. 1934. The globe thermometer in studies of heating and ventilation. *Epidemiol. Infect.* 34:458–73

Beniston M. 2004. The 2003 heat wave in Europe: a shape of things to come? An analysis based on Swiss climatological data and model simulations. *Geophys. Res. Lett.* 31:L02202

Boschat G, Simmonds I, Purich A, Cowan T, Pezza AB. 2016. On the use of composite analyses to form physical hypotheses: an example from heat wave–SST associations. *Sci. Rep.* 6:29599

Bouchama A, Mohanna FA, El-Sayed R, Eldali A, Saussereau E, et al. 2005. Experimental heatstroke in baboon: analysis of the systemic inflammatory response. *Shock* 24:332–35

Brunt D. 1943. The reactions of the human body to its physical environment. *Q. J. R. Meteorol. Soc.* 69:77–114

Budd GM. 2008. Wet-bulb globe temperature (WBGT)—its history and its limitations. *J. Sci. Med. Sport* 11:20–32

Burke MB, Hsiang SM, Miguel E. 2015. Global non-linear effect of temperature on economic production. *Nature* 527:235–39

Burke MB, Miguel E, Satyanath S, Dykema JA, Lobell DB. 2009. Warming increases the risk of civil war in Africa. *PNAS* 106:20670–74

Buzan JR, Oleson K, Huber M. 2015. Implementation and comparison of a suite of heat stress metrics within the Community Land Model version 4.5. *Geosci. Model Dev.* 8:151–70

Bynum GD, Pandolf KB, Schuette WH, Goldman RF, Lees DE, et al. 1978. Induced hyperthermia in sedated humans and the concept of critical thermal maximum. *Am. J. Physiol.-Regul. Integr. Comp. Physiol.* 235:R228–36

Byrne MP, O'Gorman PA. 2013. Link between land-ocean warming contrast and surface relative humidities in simulations with coupled climate models. *Geophys. Res. Lett.* 40:5223–27

Byrne MP, O'Gorman PA. 2016. Understanding decreases in land relative humidity with global warming: conceptual model and GCM simulations. *J. Climate* 29:9045–61

Cain B. 2006. *A Preliminary Study of Heat Strain Using Modelling and Simulation*. Toronto, Can.: Defense Research and Development Toronto (Canada)

Coffel ED, de Sherbinin A, Horton RM, Lane K, Kienberger S, Wilhelmi O. 2018. The science of adaptation to extreme heat. In *Resilience*, ed. Z Zommers, K Alverson, pp. 89–103. Cambridge, MA: Elsevier

Coumou D, Petoukhov V, Rahmstorf S, Petri S, Schellnhuber HJ. 2014. Quasi-resonant circulation regimes and hemispheric synchronization of extreme weather in boreal summer. *PNAS* 111:12331–36

Cramwinckel MJ, Huber M, Kocken IJ, Agnini C, Bijl PK, et al. 2018. New equations for computing vapor pressure and enhancement factor. *Nature* 559:382–86

Crowe J, Moya-Bonilla JM, Román-Solano B, Robles-Ramírez A. 2010. Heat exposure in sugarcane workers in Costa Rica during the non-harvest season. *Glob. Health Action* 3:5619

Crowe J, van Wendel de Joode B, Wesseling C. 2009. A pilot field evaluation on heat stress in sugarcane workers in Costa Rica: what to do next? *Glob. Health Action* 2:2062

D'Ambrosia AR, Clyde WC, Fricke HC, Gingerich PD, Abels HA. 2017. Repetitive mammalian dwarfing during ancient greenhouse warming events. *Sci. Adv.* 3:e1601430

Davies-Jones R. 2008. An efficient and accurate method for computing the wet-bulb temperature along pseudoadiabats. *Mon. Weather Rev.* 136:2764–85

Davies-Jones R. 2009. On formulas for equivalent potential temperature. *Mon. Weather Rev.* 137:3137–48

Day E, Fankhauser S, Kingsmill N, Costa H, Mavrogianni A. 2019. Upholding labour productivity under climate change: an assessment of adaptation options. *Climate Policy* 19:367–85

de Freitas CR, Grigorieva EA. 2014. A comprehensive catalogue and classification of human thermal climate indices. *Int. J. Biometeorol.* 59:109–20

Delgado Cortez O. 2009. Heat stress assessment among workers in a Nicaraguan sugarcane farm. *Glob. Health Action* 2:2069

Diffenbaugh NS, Ashfaq M. 2010. Intensification of hot extremes in the United States. *Geophys. Res. Lett.* 37:L15701

Diffenbaugh NS, Giorgi F. 2012. Climate change hotspots in the CMIP5 global climate model ensemble. *Clim. Change* 114:813–22

Diffenbaugh NS, Pal J, Giorgi F, Gao X. 2007. Heat stress intensification in the Mediterranean climate change hotspot. *Geophys. Res. Lett.* 34:L11706

Dole R, Hoerling M, Perlwitz J, Eischeid J, Pegion P, et al. 2011. Was there a basis for anticipating the 2010 Russian heat wave? *Geophys. Res. Lett.* 38:L06702

Donat MG, Pitman AJ, Seneviratne SI. 2017. Regional warming of hot extremes accelerated by surface energy fluxes. *Geophys. Res. Lett.* 44:7011–19

Dunne JP, Stouffer RJ, John JG. 2013. Reductions in labour capacity from heat stress under climate warming. *Nat. Climate Change* 3:563–66

Emanuel KA. 1995. On thermally direct circulations in moist atmospheres. *J. Atmos. Sci.* 52:1529–34

Emanuel KA, Neelin JD, Bretherton CS. 1994. On large-scale circulations in convecting atmospheres. *Q. J. R. Meteorol. Soc.* 120:1111–43

Epstein Y, Moran DS. 2006. Thermal comfort and the heat stress indices. *Ind. Health* 44:388–98

Fiala D, Lomas KJ, Stohrer M. 1999. A computer model of human thermoregulation for a wide range of environmental conditions: the passive system. *J. Appl. Physiol.* 87:1957–72
Field CB, Barros V, Stocker TF, Qin D, Dokken DJ, et al. 2012. *Managing the Risks of Extreme Events and Disasters to Advance Climate Change Adaptation: A Special Report of the Intergovernmental Panel on Climate Change*. Cambridge, UK: Cambridge Univ. Press
Fischer EM, Knutti R. 2012. Robust projections of combined humidity and temperature extremes. *Nat. Climate Change* 3:126–30
Fischer EM, Oleson KW, Lawrence DM. 2012. Contrasting urban and rural heat stress responses to climate change. *Geophys. Res. Lett.* 39:L03705
Frieling J, Gebhardt H, Huber M, Adekeye OA, Akande SO, et al. 2017. Extreme warmth and heat-stressed plankton in the tropics during the Paleocene-Eocene Thermal Maximum. *Sci. Adv.* 3:e1600891
Frierson DMW. 2006. Robust increases in midlatitude static stability in simulations of global warming. *Geophys. Res. Lett.* 33:L24816
Fyke J, Matthews HD. 2015. A probabilistic analysis of cumulative carbon emissions and long-term planetary warming. *Environ. Res. Lett.* 10:115007
Gao C, Kuklane K, Ostergren PO, Kjellstrom T. 2018. Occupational heat stress assessment and protective strategies in the context of climate change. *Int. J. Biometeorol.* 62:359–71
Garcia-Herrera R, Díaz J, Trigo RM, Luterbacher J, Fischer EM. 2010. A review of the European summer heat wave of 2003. *Crit. Rev. Environ. Sci. Technol.* 40:267–306
Gaughan J, Lacetera N, Valtorta SE, Khalifa HH, Hahn LR, Mader T. 2009. Response of domestic animals to climate challenges. In *Biometeorology for Adaptation to Climate Variability and Change*, ed. KL Ebi, pp. 131–70. Dordrecht, Neth.: Springer
Gaughan JB, Bonner SL, Loxton I, Mader TL. 2013. Effects of chronic heat stress on plasma concentration of secreted heat shock protein 70 in growing feedlot cattle. *J. Anim. Sci.* 91:120–29
Gingerich PD. 2006. Environment and evolution through the Paleocene–Eocene thermal maximum. *Trends Ecol. Evol.* 21:246–53
Goldblatt C, Robinson TD, Zahnle KJ, Crisp D. 2013. Low simulated radiation limit for runaway greenhouse climates. *Nat. Geosci.* 6:661–67
Gonzalez RR, Halford C, Keach EM. 2010. Environmental and physiological simulation of heat stroke: a case study analysis and validation. *J. Therm. Biol.* 35:441–49
Haldane JS. 1905. The influence of high air temperatures no. I. *J. Hyg.* 5:494–513
Havenith G. 1999. Heat balance when wearing protective clothing. *Ann. Occupat. Hyg.* 43:289–96
Hightower LE, Guidon PT. 1989. Selective release from cultured mammalian cells of heat-shock (stress) proteins that resemble glia-axon transfer proteins. *J. Cell. Physiol.* 138:257–66
Horton DE, Johnson NC, Singh D, Swain DL, Rajaratnam B, Diffenbaugh NS. 2015. Contribution of changes in atmospheric circulation patterns to extreme temperature trends. *Nature* 522:465–69
Houser T, Hsiang S, Kopp R, Larson K, Delgado M, et al. 2015. *Economic Risks of Climate Change: An American Prospectus*. New York: Columbia Univ. Press
Hoyos CD, Webster PJ. 2011. Evolution and modulation of tropical heating from the last glacial maximum through the twenty-first century. *Climate Dyn.* 38:1501–19
Hsiang S, Kopp R, Jina A, Rising J, Delgado M, et al. 2017. Estimating economic damage from climate change in the United States. *Science* 356:1362–69
Hsiang SM, Sobel AH. 2016. Potentially extreme population displacement and concentration in the tropics under non-extreme warming. *Sci. Rep.* 6:25697
Huber M. 2008. A hotter greenhouse? *Science* 321:353–54
Huber V, Ibarreta D, Frieler K. 2017. Cold- and heat-related mortality: a cautionary note on current damage functions with net benefits from climate change. *Clim. Change* 142:407–18
Hurley JV, Boos WR. 2015. A global climatology of monsoon low-pressure systems. *Q. J. R. Meteorol. Soc.* 141:1049–64
Hyatt OM, Lemke B, Kjellstrom T. 2010. Regional maps of occupational heat exposure: past, present, and potential future. *Glob. Health Action* 3:741

Im ES, Kang S, Eltahir EAB. 2018. Projections of rising heat stress over the western maritime continent from dynamically downscaled climate simulations. *Glob. Planet. Change* 165:160–72
Im ES, Pal JS, Eltahir EAB. 2017. Deadly heat waves projected in the densely populated agricultural regions of South Asia. *Sci. Adv.* 3:e1603322
Ito K, Lane K, Olson C. 2018. Equitable access to air conditioning: a city health department's perspective on preventing heat-related deaths. *Epidemiology* 29:749–52
Jendritzky G, Tinz B. 2009. The thermal environment of the human being on the global scale. *Glob. Health Action* 2:2005
Kang S, Eltahir EAB. 2018. North China plain threatened by deadly heatwaves due to climate change and irrigation. *Nat. Commun.* 9:2894
Kasai M, Okaze T, Mochida A, Hanaoka K. 2017. Heatstroke risk predictions for current and near-future summers in Sendai, Japan, based on mesoscale WRF simulations. *Sustainability* 9:1467
Kelley CP, Mohtadi S, Cane MA, Seager R, Kushnir Y. 2015. Climate change in the Fertile Crescent and implications of the recent Syrian drought. *PNAS* 112:3241–46
Kjellstrom T, Briggs D, Freyberg C, Lemke B, Otto M, Hyatt O. 2016. Heat, human performance, and occupational health: a key issue for the assessment of global climate change impacts. *Annu. Rev. Public Health* 37:97–112
Kjellstrom T, Holmer I, Lemke B. 2009a. Workplace heat stress, health and productivity—an increasing challenge for low and middle-income countries during climate change. *Glob. Health Action* 2:2047
Kjellstrom T, Kovats RS, Lloyd SJ, Holt T, Tol RS. 2009b. The direct impact of climate change on regional labor productivity. *Arch. Environ. Occup. Health* 64:217–27
Kjellstrom T, Lemke B, Otto M. 2013. Mapping occupational heat exposure and effects in South-East Asia: ongoing time trends 1980–2011 and future estimates to 2050. *Ind. Health* 51:56–67
Kjellstrom T, Mercado S. 2008. Towards action on social determinants for health equity in urban settings. *Environ. Urban.* 20:551–74
Kobayashi S, Ota Y, Harada Y, Ebita A. 2015. The JRA-55 reanalysis: general specifications and basic characteristics. *J. Meteorol. Soc. Jpn.* 93:5–48
Komurcu M, Emanuel K, Huber M, Acosta R. 2018. High-resolution climate projections for the northeastern United States using dynamical downscaling at convection-permitting scales. *Earth Space Sci.* 5:801–26
Koppe C, Kovats S, Jendritzky G, Menne B. 2004. *Heat-Waves: Risks and Responses.* Copenhagen, Den.: World Health Organ.
Korty RL, Emanuel KA, Huber M, Zamora RA. 2017. Tropical cyclones downscaled from simulations with very high carbon dioxide levels. *J. Climate* 30:649–67
Korty RL, Schneider T. 2007. A climatology of the tropospheric thermal stratification using saturation potential vorticity. *J. Climate* 20:5977–91
Kovats RS, Hajat S. 2008. Heat stress and public health: a critical review. *Annu. Rev. Public Health* 29:41–55
Kraning KK, Gonzalez RR. 1997. A mechanistic computer simulation of human work in heat that accounts for physical and physiological effects of clothing, aerobic fitness, and progressive dehydration. *J. Therm. Biol.* 22:331–42
Kuehn LA, Stubbs RA, Weaver RS. 1970. Theory of the globe thermometer. *J. Appl. Physiol.* 29:750–57
Kumar R, Mishra V, Buzan J, Kumar R, Shindell D, Huber M. 2017. Dominant control of agriculture and irrigation on urban heat island in India. *Sci. Rep.* 7:14054
Lauwaet D, Hooyberghs H, Maiheu B, Lefebvre W, Driesen G, et al. 2015. Detailed urban heat island projections for cities worldwide: dynamical downscaling CMIP5 global climate models. *Climate* 3:391–415
Lehmann J, Coumou D. 2015. The influence of mid-latitude storm tracks on hot, cold, dry and wet extremes. *Sci. Rep.* 5:17491
Li B, Sain S, Mearns L, Anderson H, Kovats S, et al. 2012. The impact of extreme heat on morbidity in Milwaukee, Wisconsin. *Clim. Change* 110:959–76
Li J, Chen YD, Gan TY, Lau NC. 2018. Elevated increases in human-perceived temperature under climate warming. *Nat. Climate Change* 8:43–47
Liljegren JC, Carhart RA, Lawday P, Tschopp S, Sharp R. 2008. Modeling the wet bulb globe temperature using standard meteorological measurements. *J. Occup. Environ. Hyg.* 5:645–55

Liu X, Tang Q, Liu W, Yang H, Groisman P, et al. 2019. The asymmetric impact of abundant preceding rainfall on heat stress in low latitudes. *Environ. Res. Lett.* 14:044010
Lu Y, Kueppers L. 2015. Increased heat waves with loss of irrigation in the United States. *Environ. Res. Lett.* 10:064010
Margolis HG. 2014. Heat waves and rising temperatures: human health impacts and the determinants of vulnerability. In *Global Climate Change and Public Health*, ed. KE Pinkerton, WN Rom, pp. 85–120. New York: Springer
Masterson JM, Richardson FA. 1979. *Humidex: A Method of Quantifying Human Discomfort Due to Excessive Heat and Humidity*. Downsview, Can.: Atmospheric Environment
Matthews T. 2018. Humid heat and climate change. *Progress Phys. Geogr.-Earth Environ.* 42:391–405
Matthews TKR, Wilby RL, Murphy C. 2017. Communicating the deadly consequences of global warming for human heat stress. *PNAS* 114:3861–66
McCarthy MP, Best MJ, Betts RA. 2010. Climate change in cities due to global warming and urban effects. *Geophys. Res. Lett.* 37:L09705
McGregor GR, Vanos JK. 2018. Heat: a primer for public health researchers. *Public Health* 161:138–46
McKinnon KA, Rhines A, Tingley MP, Huybers P. 2016. Amplified mid-latitude planetary waves favour particular regional weather extremes. *Nat. Geosci.* 9:389
Meehl GA, Tebaldi C. 2004. More intense, more frequent, and longer lasting heat waves in the 21st century. *Science* 305:994–97
Minard D, Belding HS, Kingston JR. 1957. Prevention of heat casualties. *J. Am. Med. Assoc.* 165:1813–18
Mitchell D, Fuller A, Maloney SK. 2009. Homeothermy and primate bipedalism: Is water shortage or solar radiation the main threat to baboon (*Papio hamadryas*) homeothermy? *J. Hum. Evol.* 56:439–46
Mitchell D, Maloney S, Jessen C, Laburn H, Kamerman P, et al. 2002. Adaptive heterothermy and selective brain cooling in arid-zone mammals. *Comp. Biochem. Physiol. B: Biochem. Mol. Biol.* 131:571–85
Mitchell D, Snelling EP, Hetem RS, Maloney SK, Strauss WM, Fuller A. 2018. Revisiting concepts of thermal physiology: predicting responses of mammals to climate change. *J. Anim. Ecol.* 87:956–73
Monteiro A, Carvalho V, Velho S, Sousa C. 2013. The accuracy of the heat index to explain the excess of mortality and morbidity during heat waves—a case study in a Mediterranean climate. *Bull. Geogr. Soc.-Econ. Ser.* 20:71–84
Moore FC, Baldos U, Hertel T, Diaz D. 2017. New science of climate change impacts on agriculture implies higher social cost of carbon. *Nat. Commun.* 8:1607
Mora C, Counsell CWW, Bielecki CR, Louis LV. 2017a. Twenty-seven ways a heat wave can kill you: deadly heat in the era of climate change. *Circ.-Cardiovasc. Q. Outcomes* 10:e004233
Mora C, Dousset B, Caldwell IR, Powell FE, Geronimo RC, et al. 2017b. Global risk of deadly heat. *Nat. Climate Change* 7:501–6
Nilsson M, Kjellstrom T. 2010. Climate change impacts on working people: how to develop prevention policies. *Glob. Health Action* 3:1543
O'Donnell J, Tobey M, Weiner D, Stevens L, Johnson S, et al. 2011. Prevalence of and risk factors for chronic kidney disease in rural Nicaragua. *Nephrol. Dial. Transplant.* 26:2798–805
O'Neill M, Zanobetti A, Schwartz J. 2003. Modifiers of the temperature and mortality association in seven US cities. *Am. J. Epidemiol.* 157:1074–82
Oppermann E, Strengers Y, Maller C, Rickards L, Brearley M. 2018. Beyond threshold approaches to extreme heat: repositioning adaptation as everyday practice. *Weather Climate Soc.* 10:885–98
Pal JS, Eltahir EA. 2016. Future temperature in southwest Asia projected to exceed a threshold for human adaptability. *Nat. Climate Change* 6:197–200
Pandolf K, Kamon E. 1974. Respiratory responses to intermittent and prolonged exercise in a hot-dry environment. *Life Sci.* 14:187–98
Parsons K. 2006. Heat stress standard ISO 7243 and its global application. *Ind. Health* 44:368–79
Petoukhov V, Petri S, Rahmstorf S, Coumou D, Kornhuber K, Schellnhuber HJ. 2016. Role of quasiresonant planetary wave dynamics in recent boreal spring-to-autumn extreme events. *PNAS* 113:6862–67
Petoukhov V, Rahmstorf S, Petri S, Schellnhuber HJ. 2013. Quasiresonant amplification of planetary waves and recent Northern Hemisphere weather extremes. *PNAS* 110:5336–41

Pierrehumbert RT. 1995. Thermostats, radiator fins, and the local runaway greenhouse. *J. Atmos. Sci.* 52:1784–806

Platt M, Vicario S. 2013. Heat illness. In *Rosen's Emergency Medicine—Concepts and Clinical Practice*, ed. J Marx, R Walls, R Hockberger, pp. 1896–905. Philadelphia, PA: Elsevier

Randell H, Gray C. 2019. Climate change and educational attainment in the global tropics. *PNAS* 116:8840–45

Ratnam JV, Behera SK, Ratna SB, Rajeevan M, Yamagata T. 2016. Anatomy of Indian heatwaves. *Sci. Rep.* 6:24395

Raymond C, Singh D, Horton RM. 2017. Spatiotemporal patterns and synoptics of extreme wet-bulb temperature in the contiguous United States. *J. Geophys. Res. Atmos.* 122:13108–24

Robine JM, Cheung SLK, Le Roy S, Van Oyen H, Griffiths C, et al. 2008. Death toll exceeded 70,000 in Europe during the summer of 2003. *C. R. Biol.* 331:171–78

Rogers JC. 2013. The 20th century cooling trend over the southeastern United States. *Climate Dyn.* 40:341–52

Ross ME, Vicedo-Cabrera AM, Kopp RE, Song L, Goldfarb DS, et al. 2018. Assessment of the combination of temperature and relative humidity on kidney stone presentations. *Environ. Res.* 162:97–105

Rothfusz L. 1990. *The heat index equation (or, more than you ever wanted to know about heat index).* Tech. Attach. SR 90-23, Natl. Weather Serv., Fort Worth, TX

Russo S, Sillmann J, Sterl A. 2017. Humid heat waves at different warming levels. *Sci. Rep.* 7:7477

Schär C. 2015. The worst heat waves to come. *Nat. Climate Change* 6:128–29

Schleussner CF, Donges JF, Donner RV, Schellnhuber HJ. 2016. Armed-conflict risks enhanced by climate-related disasters in ethnically fractionalized countries. *PNAS* 113:9216–21

Screen JA, Simmonds I. 2014. Amplified mid-latitude planetary waves favour particular regional weather extremes. *Nat. Climate Change* 4:704–9

Semenza JC, Rubin CH, Falter KH, Selanikio JD, Flanders WD, et al. 1996. Heat-related deaths during the July 1995 heat wave in Chicago. *N. Engl. J. Med.* 335:84–90

Seneviratne SI, Nicholls N, Easterling D, Goodess CM, Kanae S, et al. 2012. Changes in climate extremes and their impacts on the natural physical environment. In *Managing the Risks of Extreme Events and Disasters to Advance Climate Change Adaptation*, ed. CB Field, V Barros, TF Stocker, Q Dahe, DJ Dokken, et al., pp. 109–230. New York: Cambridge Univ. Press

Sheffield P, Herrera J, Lemke B, Kjellstrom T, Romero L. 2013. Current and future heat stress in Nicaraguan work places under a changing climate. *Ind. Health* 51:123–27

Sherwood SC. 2018. How important is humidity in heat stress? *J. Geophys. Res. Atmos.* 123:11808–10

Sherwood SC, Huber M. 2010. An adaptability limit to climate change due to heat stress. *PNAS* 107:9552–55

Sillmann J, Kharin VV, Zwiers FW, Zhang X, Bronaugh D. 2013. Climate extremes indices in the CMIP5 multimodel ensemble: part 2. Future climate projections. *J. Geophys. Res. Atmos.* 118:2473–93

Simon H. 1993. Hyperthermia. *N. Engl. J. Med.* 329:483–87

Smith KR, Woodward A, Lemke B, Otto M, Chang CJ, et al. 2016. The last Summer Olympics? Climate change, health, and work outdoors. *Lancet* 388:642–44

Smith T, Itterbeeck JV, Missiaen P. 2004. Oldest Plesiadapiform (Mammalia, Proprimates) from Asia and its palaeobiogeographical implications for faunal interchange with North America. *C. R. Palevol* 3:43–52

Speakman JR, Król E. 2010. Maximal heat dissipation capacity and hyperthermia risk: neglected key factors in the ecology of endotherms: heat dissipation limit theory. *J. Anim. Ecol.* 79:726–46

Speakman JR, Król E. 2011. Limits to sustained energy intake. XIII. Recent progress and future perspectives. *J. Exp. Biol.* 214:230–41

St-Pierre N, Cobanov B, Schnitkey G. 2003. Economic losses from heat stress by US livestock industries. *J. Dairy Sci.* 86:E52–77

Steadman RG. 1979. The assessment of sultriness. Part I: a temperature-humidity index based on human physiology and clothing science. *J. Appl. Meteorol.* 18:861–73

Stolwijk JA. 1971. *A mathematical model of physiological temperature regulation in man.* NASA Contract. Rep. CR-1855, Washington, DC

Tattersall GJ, Sinclair BJ, Withers PC, Fields PA, Seebacher F, et al. 2012. Coping with thermal challenges: physiological adaptations to environmental temperatures. *Compr. Physiol.* 2:2151–202

Taylor KE, Stouffer RJ, Meehl GA. 2012. An overview of CMIP5 and the experiment design. *Bull. Am. Meteorol. Soc.* 93:485–98

Teng H, Branstator G, Meehl GA, Washington WM. 2016. Projected intensification of subseasonal temperature variability and heat waves in the Great Plains. *Geophys. Res. Lett.* 43:2165–73

Teng H, Branstator G, Wang H, Meehl GA, Washington WM. 2013. Probability of US heat waves affected by a subseasonal planetary wave pattern. *Nat. Geosci.* 6:1056–61

van Hooidonk R, Huber M. 2009. Equivocal evidence for a thermostat and unusually low levels of coral bleaching in the Western Pacific Warm Pool. *Geophys. Res. Lett.* 36:L06705

Wang Y, Nordio F, Nairn J, Zanobetti A, Schwartz JD. 2018. Accounting for adaptation and intensity in projecting heat wave-related mortality. *Environ. Res.* 161:464–71

Weber S, Sadoff N, Zell E, de Sherbinin A. 2015. Policy-relevant indicators for mapping the vulnerability of urban populations to extreme heat events: a case study of Philadelphia. *Appl. Geogr.* 63:231–43

Whitman S, Good G, Donoghue ER, Benbow N, Shou W, Mou S. 1997. Mortality in Chicago attributed to the July 1995 heat wave. *Am. J. Public Health* 87:1515–18

Willett KM, Sherwood S. 2010. Exceedance of heat index thresholds for 15 regions under a warming climate using the wet-bulb globe temperature. *Int. J. Climatol.* 32:161–77

Williams IN, Pierrehumbert RT. 2017. Observational evidence against strongly stabilizing tropical cloud feedbacks. *Geophys. Res. Lett.* 44:1503–10

Williams IN, Pierrehumbert RT, Huber M. 2009. Global warming, convective threshold and false thermostats. *Geophys. Res. Lett.* 36:L21805

Wu Y, Pauluis O. 2014. Midlatitude tropopause and low-level moisture. *J. Atmos. Sci.* 71:1187–200

Wu Y, Pauluis O. 2015. What is the representation of the moisture–tropopause relationship in CMIP5 models? *J. Climate* 28:4877–89

Wyndham CH, Atkins AR. 1968. A physiological scheme and mathematical model of temperature regulation in man. *Pflügers Arch.* 303:14–30

Yang J, Wang ZH, Kaloush KE. 2015. Environmental impacts of reflective materials: Is high albedo a silver bullet for mitigating urban heat island? *Renew. Sustain. Energy Rev.* 47:830–43

Yokota M, Berglund L, Cheuvront S, Santee W, Latzka W, et al. 2008. Thermoregulatory model to predict physiological status from ambient environment and heart rate. *Comput. Biol. Med.* 38:1187–93

Zamora RA, Korty RL, Huber M. 2016. Thermal stratification in simulations of warm climates: a climatology using saturation potential vorticity. *J. Climate* 29:5083–102

Zhao Y, Ducharne A, Sultan B, Braconnot P, Vautard R. 2015. Estimating heat stress from climate-based indicators: present-day biases and future spreads in the CMIP5 global climate model ensemble. *Environ. Res. Lett.* 10:084013